

# Discovery of Quasi-Integrable Equations from traveling-wave data using the Physics-Informed Neural Networks

A. Nakamura,<sup>1,\*</sup> K. Obuse,<sup>2,†</sup> N. Sawado,<sup>3,‡</sup> K. Shimasaki,<sup>3,§</sup>  
 Y. Shimazaki,<sup>3,¶</sup> Y. Suzuki,<sup>3,\*\*</sup> and K. Toda<sup>4,5,††</sup>

<sup>1</sup>*Department of Physics, School of Science,  
 Kitasato University, Sagami-hara, Kanagawa 252-0373, Japan*

<sup>2</sup>*Graduate School of Natural Science and Technology,  
 Okayama University, Okayama 700-8530, Japan*

<sup>3</sup>*Department of Physics and Astronomy, Tokyo University of Science, Noda, Chiba 278-8510, Japan*

<sup>4</sup>*Department of Mathematical Physics, Toyama Prefectural University, Imizu, Toyama 939-0398, Japan*

<sup>5</sup>*Research and Education Center for Natural Sciences, Keio University,  
 Hiyoshi 4-1-1, Yokohama, Kanagawa 223-8521, Japan*

Physics-Informed Neural Networks (PINNs) have emerged as a powerful tool for analyzing nonlinear partial differential equations and identifying governing equations from observational data. In this study, we apply PINNs to investigate vortex-type solutions of quasi-integrable equations in two spatial dimensions, specifically the Zakharov-Kuznetsov (ZK) and the Regularized Long-Wave (RLW) equations. These equations are toy models for geostrophic shallow water dynamics in planetary atmospheres. We first demonstrate that PINNs can successfully solve these equations in the forward process using a mesh-free approach with automatic differentiation. However, in the inverse process, substantial misidentification occurs due to the structural similarities between the ZK and the RLW equations. To address this issue, we then introduce conservation law-enhanced PINNs, initial condition variations, and a friction-based perturbation approach to improve identification accuracy. Our results show that incorporating small perturbations while preserving conservation laws significantly enhances the resolution of equation identification. These findings may contribute to the broader goal of using deep learning techniques for discovering governing equations in complex fluid dynamical systems, such as Jupiter’s Great Red Spot.

---

\* nakamura@sci.kitasato-u.ac.jp

† obuse@okayama-u.ac.jp

‡ sawadoph@rs.tus.ac.jp

§ shimasakitus@gmail.com

¶ shimazakitus@gmail.com

\*\* ytszkyuta@gmail.com

†† kouichi@yukawa.kyoto-u.ac.jp

## I. INTRODUCTION

Non-linear wave phenomena widely appear in various physical systems with different scales, such as particle physics, condensed matter, biological problems, and planetary atmospheres. We believe that each phenomenon can be described by suitable partial differential equations (PDEs). Non-linear PDEs that admit soliton solutions are of special interest because of their mathematical beauty and consistency, i.e., their integrability. It supports properties such as the solutions having an infinite number of conservation laws, Painlevé properties, reducibility into bilinear forms. Probably, the most well-known equation with these properties is the Korteweg-de Vries (KdV) equation

$$u_t + u_x + 2uu_x + u_{xxx} = 0, \quad (1)$$

describing shallow water waves in 1+1 dimensions. Note that the second term of (1) is removed by taking  $x' = x - t$  and  $t$  as independent time variables. Zabusky and Kruskal made the first observations of the basic property of the solitons in the equation [1]. On the other hand, Benjamin, Bona, and Mahony argued the superiority of the regularized long-wave (RLW) equation

$$u_t + u_x + 2uu_x - u_{xxt} = 0 \quad (2)$$

over (1) for describing long-wave nature [2]. They claimed these equations are known to be equivalent in the zeroth order,  $u_t = -u_x$  of their perturbation. However, significant differences appear concerning these neighboring equation's essential mathematical and numerical aspects. Here, a natural question arises: if numerical data is given from an observation, how do we identify the appropriate governing equation?

Then, this paper concerns the identification of two 2+1 dimensional quasi-integrable equations, the Zakharov-Kuznetsov (ZK) equation and the RLW equation, which are supposed to be toy models of the shallow-water equations. The ZK equation given by [3, 4]

$$u_t + 2uu_x + (\nabla^2 u)_x = 0 \quad (3)$$

is a direct extension of the KdV equation into higher dimensions. To date, most of the previous research [4–6] are focused on the 2 + 1 dimensional version of the model. The equation possesses stable isolated vortex-type solutions which enjoy solitonic properties. It is well known that some inelastic properties emerge in a collision process when the strengths of vortices are significantly different, the taller soliton gains more height while the shorter one tends to wane with radiation [4]. The RLW equation [2, 7] is a shallow-water fluid model to simulate the development of an undular

bore. The RLW equation in 2 + 1 dimensions

$$u_t + u_x + uu_x - (\nabla^2 u)_t = 0 \quad (4)$$

possesses a stable isolated vortex solution [8]. The peculiar inelastic properties of the solitons have been extensively studied in the literatures [9–11] in 1+1 dimensions and also [8] in 2+1 dimensions. Stable fluid mechanical vortices in shallow water equations are often discussed in the context of quasi-integrable equations in 2+1 dimensions. Notably, the significant dynamics of planetary atmospheres of Jupiter's or other planets are described by some non-linear PDEs in 2 or 3 spatial dimensions. The Great Red Spot (GRS) of Jupiter is an illustration of a unique, extraordinary object because of its fantastic longevity. Many observations indicate that the phenomenon is undoubtedly shallow [12]. Its stable nature strongly suggests that there exists unknown mechanics coming from the highly non-linear nature of dynamics. Models of shallow water equations and (or) their induced effective equations in several geostrophic regimes may describe the physics of the GRS. In the quasi-geostrophic regime, the Charney-Hasegawa-Mima (CHM) equation [13] and the drift-wave equation [14] by including the scalar non-linear term  $uu_x$

$$(1 - \nabla^2)u_t + u_x - J[u, \nabla^2 u] = 0, \quad (5)$$

$$(1 - \nabla^2)u_t + u_x + uu_x - J[u, \nabla^2 u] = 0, \quad (6)$$

respectively, are proposed, where the last term in equations, the Jacobian, is defined as  $J[A, B] := (\partial_x A)(\partial_y B) - (\partial_y A)(\partial_x B)$ . These equations possess the vortex solutions with the dipole (CHM) and the monopole (drift-wave). In the intermediate geostrophic regime, the governing equation called Williams-Yamagata-Flierl (WYF) equation [15–17] (in cyclonic shear) is defined as

$$u_t + 2uu_x + P(y)(\nabla^2 u)_x + 2Q(y)u_x + 2J[u, \nabla^2 u] = 0, \quad (7)$$

$$P(y) = 1 + 2u^0(y), Q(y) = y + u_{yy}^0 + \int^y u_0(y') dy', \quad (8)$$

where  $u^0$  provides the effect of the background shear flow. With such various model equations in hand, the crucial step in solving a physical problem is to choose the appropriate governing equation. There are numerous potential possibilities for describing the GRS, but we are aware that the most appropriate equation for those phenomena is still unclear. Discovery of the governing equation is thus crucial because it determines an appropriate physical regime for the phenomenon. At present, the observation data is still not enough to discover the equation for many phenomena including GRS. Thus, we do not go into realistic models (CHM, WYF), and focus on the toy models of

these equations. Within a simple approximation  $J \sim 0$ <sup>1</sup> the ZK and RLW equations can be toy models of the geostrophic equations. For the ZK equation, a shear flow  $u^0 = -1$  [17] must be chosen. We believe that analysis of the identification in these equations will eventually be useful for determining geostrophic regimes of the above significant atmospheric problems.

We study the identification of non-linear PDEs by means of deep learning technology. The application of deep learning in deep neural networks to non-linear PDEs has recently gained much attention. The Physics-Informed Neural Networks (PINNs) [18–20] have the ability to solve many complicated scientific problems, such as fluid and solid mechanics [21–26], cyber-physical systems [27], biological systems [28–31], and many others. Since the methods’ original premise involved an application to fluid mechanics with PDEs [21, 22] and a weather/climate modelling [25], it is natural to extend the analysis into the significant dynamics of planetary atmospheres described by some PDEs. One unique, noteworthy aspect of the PINNs is their ability to solve PDEs (the forward analysis) efficiently and also to provide us with an accurate estimate of the equation based on the governing data of the physical problems of our concern (the inverse analysis). PINNs generally have significantly higher extrapolation power than other conventional deep-learning techniques, making them appropriate for analyses involving limited learning data. In [32, 33], Sivalingam et al. have proposed sophisticated methods for solving several fractional-order PDEs. Recently, there have been some attempts to apply the methods to the more complex geometry of data [34, 35].

In the present paper, we solve quasi-integrable equations via PINNs as reduced toy models instead of directly solving above-mentioned geostrophic equations. The above geostrophic equations give us many insights into the phenomena, and the traditional approaches can, of course, work for the analysis of these equations. One advantage of solving the integrable equations or the quasi-integrable counterparts is to expose the corresponding phenomena and a primary character usually described by some mathematical language such as the existence of (infinite number of) conservation quantities. There are numerous studies of PINNs for the integrable equations, such as the Burgers equation [18–20, 36, 37], the KdV equation and the modified KdV equation [37–42], the non-linear Schrödinger equation [43, 44], and many other variations. However, only few analyses have been studied in 2+1 dimensions. There are the PINN analysis for the line solitons of the integrable Kadomtsev-Petviashvili equation [45] and also of the non-linear Schrödinger equation [46, 47]. The stationary vortex solutions in the nonlinear Schrödinger equation were studied in [48]. To our knowledge, no concrete research has yet been done on the ZK or the RLW equations. It should

---

<sup>1</sup> For the solutions enjoying circular symmetry, the Jacobian is always zero. Note that our solutions in the present paper sometimes deviate from the circular shape.

be noted that PINNs are distinct from the conventional, standard numerical algorithm [37, 49–52] that uses the finite difference and finite element methods, where the governing PDEs are eventually discretized over the computational domain. Providing a mesh-free approach is one of the main benefits of PINNs since automatic differentiation approximates the differential operators in the governing PDEs. Traditional numerical approaches strongly depend on grid settings, which may cause a curse of dimensionality. On the other hand, PINN grid independence is undoubtedly efficient, particularly for solving high-dimensional problems and inverse analysis. A notable feature of these higher dimensional non-linear PDE is the quasi-integrable property, where a limited number of conservation quantities exist, or they tend to be broken in some situations such as during the inelastic collision [53]. Thus, it is worth using the PINNs that can realize conservation quantities. A benefit of utilizing PINNs is their ability to integrate the conservation laws of a system into analysis by incorporating the condition into the loss function. The method called cPINNs gains the accuracy of the analysis [36, 37, 54].

Data-driven discovery in the present paper is the inverse analysis of parameter inference of the governing equations. The procedure is as follows:(i) We numerically solve the quasi-integrable equations using the standard algorithm such as the Runge-Kutta method, or PINNs. (ii) Using these data, we perform the PINN’s inverse analysis to determine the coefficients of the equations and to see how the proper equation is identified. The PINN inverse analysis may result in substantial misidentification between the vortex solutions of the ZK and the RLW equations. That is, when the candidate equation has terms from both the ZK and the RLW equations, the inverse PINNs cannot determine the governing equation. These equations have a lot in common. For example, they have the same number of conserved quantities and possess the same form of traveling wave solution. It appears to be the origin of the substantial misidentification that could happen in PINN inverse analysis. The present paper provides several tentative resolutions for avoiding the problem.

For the PDE discovery, a sparse learning algorithm [55–57] is quite efficient for getting proper information on the structure of the governing equation. The procedure is as follows. Firstly, one selects feasible candidates for the corresponding problem, and then we refine them to select the most appropriate equation using PINNs. With the equation we consider here because of their dimensionality, the degrees of freedom of the problem become large, thus carrying out the first part of the algorithms is very hard. Therefore, in the present paper, we concentrate on the second part, i.e., just the PINN analysis.

The present paper is based on the proceedings paper of *the XII. International Symposium on Quantum Theory and Symmetries (QTS12)* [58]. In the proceedings, we presented a few potential

solutions to the problem, including variations of the initial conditions and a friction method in terms of the  $y$ -dependent sheared current, which will be thoroughly covered in the present paper. The approach is undoubtedly improved in this paper, and we obtain excellent convergent properties of the mean-squared error, which was not looked at in the previous study. In this paper, we will introduce a new friction that improves the identification ability compared to the method shown in the proceedings. We also focus on the cPINN analysis and the use of the two-soliton solutions for the inverse analysis, which are the inventive contents of the present paper.

The paper is organized as follows. In Section II, we give a brief introduction to the ZK and the RLW equations. The conservation quantities in these equations are derived in this section. We present an overview of PINNs in Section III. We demonstrate the misidentification of the solutions as well as the good performance of PINNs for the quasi-integrable equations. We provide several (less effective) prescriptions to avoid the problem. In Section IV, we give successful solutions introducing variations of the initial conditions and a small perturbation for the equations and showing how they work well. The conclusions and remarks are presented in the last section.

## II. (2 + 1)DIMENSIONAL QUASI-INTEGRABLE SYSTEMS AND THE STABLE VORTICES

Though the term “quasi-integrability” is frequently employed in literature, it is still obscure mathematically. One nice, straightforward definition of a quasi-integrable system is a PDE that has only a finite number of exact conserved quantities<sup>2</sup>. The quasi-integrable systems we investigate in this paper are based on the simple definition above. Their solutions resemble solitons in the integrable system and have just four conservation quantities. This paper investigates a well-known quasi-integrable system in two space dimensions that embody the underlying KdV dynamics for the stability of their vortex solutions. The PINN analysis detects a signal resulting from partial conservation of the quantities, which will be seen in the next section.

### A. THE ZAKHAROV-KUZNETSOV EQUATION

The ZK equation

$$\frac{\partial u}{\partial t} + 2u \frac{\partial u}{\partial x} + \frac{\partial}{\partial x} (\nabla^2 u) = 0, \quad (9)$$

---

<sup>2</sup> In [11, 59], the authors give more thorough discussions about the concept of quasi-integrability.

originally was the model for the plasma dynamics in three dimensions with a uniform magnetic field [3]. Since most of the later research [4–6] have focused on the two-dimensional version of the model, the Laplacian specifies  $\nabla^2 = \partial_x^2 + \partial_y^2$ . Eq.(9) possesses meta-stable isolated vortex-type solutions which enjoy the solitonic properties. The single soliton is dynamically stable, and the two solitons of almost same height appears to collide without merging or dissipating, similar to the well-known collision properties of the KdV solitons. This does not apply to the two solitons whose heights are significantly different. The taller soliton is amplified while the shorter one tends to wane with the radiation [4].

The solutions of (9) propagate in a specific direction with uniform speeds. Here, we set the direction in the positive  $x$  orientation and velocity as  $c$ , namely assuming  $u = U(\tilde{x} := x - ct, y)$ . Plugging it into (9), we obtain

$$\nabla^2 U = cU - U^2, \quad (10)$$

where  $\nabla^2 = \partial_{\tilde{x}}^2 + \partial_y^2$ . A steady progressive exact wave solution is of the form

$$U_{1d} = \frac{3c}{2} \operatorname{sech}^2 \left[ \frac{\sqrt{c}}{2} (\tilde{x} \cos \theta + y \sin \theta) \right], \quad (11)$$

where the  $\theta$  is a given inclined angle of the solution. It indicates that this solution is just a trivial embedding of the KdV soliton into two spatial dimensions. There are several mathematical and computational achievements. On the other hand, (10) possesses another solution keeping circular symmetry (11). To find it, we introduce cylindrical coordinates and rewrite the equation as

$$\frac{1}{r} \frac{d}{dr} \left( r \frac{dU(r)}{dr} \right) = cU(r) - U(r)^2, \quad (12)$$

where  $r := \sqrt{\tilde{x}^2 + y^2}$ . We can find the solutions with the boundary condition  $U \rightarrow 0$  as  $r \rightarrow \infty$  numerically, and the solutions form a one-parameter family of  $c$  such as  $U(r) := cF(\sqrt{c}r)$ .

The solutions of (9) exhibit soliton-like properties; however, they are not similar to the solitons in integrable systems such as those of the KdV equation, and the stability of the solutions may be supported by the infinite number of conserved quantities in the equation. Eq.(9) admits only the four integrals of motion [60], which are

$$I_1 := \int i_1(y) dy = \int u dx dy, \quad i_1(y) := \int u dx, \quad (13)$$

$$I_2 := \int \frac{1}{2} u^2 dx dy, \quad (14)$$

$$I_3 := \int \left[ \frac{1}{2} (\nabla u)^2 - \frac{1}{3} u^3 \right] dx dy, \quad (15)$$

$$I_4 := \int \mathbf{r} u dx dy - t e_x \int u^2 dx dy, \quad (16)$$

where  $\mathbf{r}$  and  $\mathbf{e}_x$  are the two-dimensional position vector and the unit vector in the  $x$ -direction. Here,  $I_1$  is interpreted as the “mass” of the solution, and  $I_1(y)$  itself is conserved similarly to the case of the KdV equation. Also,  $I_2, I_3, I_4$  means the momentum, the energy, and the center of mass, respectively. We, therefore, conclude that the ZK equation is not an integrable system in the manner of ordinary soliton equations.

There are several stability studies of the line solitons [61, 62], and particularly of the transverse instability in [63, 64]. For the other type of solitons such as the bell-shaped solitary waves with circular symmetry, the stability analysis was extensively studied in [65]. Also, some transitions from the line soliton to the bell-shaped solitons were observed [66, 67]. Some discussions, including the stability property, are also given in [60].

## B. The regularized long-wave equation

The RLW equation was introduced by Peregrine [7] to simulate the development of the undular bore in the shallow water system, and many analytical and numerical studies have followed it such as [2, 8, 68–72]. The two-dimensional version of the RLW equation

$$\frac{\partial u}{\partial t} + \frac{\partial u}{\partial x} + u \frac{\partial u}{\partial x} - \frac{\partial}{\partial t} (\nabla^2 u) = 0 \quad (17)$$

concerns the drift waves in magnetized plasma or the Rossby waves in rotating fluids, where the field  $u$  describes the mean horizontal velocity of the water. Our aim in the present paper is to mainly clarify the effects of the third-order derivatives terms  $u_{xxx}$  in the ZK equation and  $u_{xxt}$  in the RLW equation. For simplifying the discussion, instead of (17), we employ

$$\frac{\partial u}{\partial t} + u \frac{\partial u}{\partial x} - \frac{\partial}{\partial t} (\nabla^2 u) = 0, \quad (18)$$

with removal of the term  $u_x$  from (17). It is merely a practical reason for the omission. As we will see in the next section, the misidentification problem occurs when we examine the inverse problem using the PINNs with the terms  $u_{txx}, u_{xxx}$  in the equations. Furthermore, adding  $u_x$  to (9) and (18) causes an additional identification problem that might happen between  $u_t$  and  $u_x$ , which complicates the problem. It is straightforward to see that the modified equation (18) also possesses the steady traveling solutions like (17), which we shall see in the following. For the steady traveling solutions, the ZK and the RLW equations have similar fundamental properties. By plugging  $u = U(\tilde{x}, y)$  into (17) or (18), we promptly get

$$c \nabla^2 U = (c - 1)U - \frac{1}{2}U^2 \quad (19)$$

or

$$c \nabla^2 U = cU - \frac{1}{2}U^2. \quad (20)$$

The transformations of the fields leads

$$\text{the ZK equation (9): } U = cF(X, Y), \quad X := \sqrt{c} \tilde{x}, \quad Y := \sqrt{c} y, \quad (c > 0) \quad (21)$$

$$\text{the RLW equation (17): } U = 2(c-1)F(X, Y), \quad X := \sqrt{1 - \frac{1}{c}} \tilde{x}, \quad Y := \sqrt{1 - \frac{1}{c}} y, \\ (c > 1, c < 0)$$

$$\text{the modified RLW equation (18): } U = 2cF(X, Y), \quad X := \tilde{x}, \quad Y := y, \quad (22)$$

we promptly get a normalized identical equation

$$\nabla^2 F - F + F^2 = 0, \quad \nabla^2 := \partial_X^2 + \partial_Y^2. \quad (23)$$

As we have already stated, (23) possesses the traveling-wave solution (like (11)) or the circular symmetric solution. Our central concern in the paper is that coincidence of transformed equations ((9)), ((17)) and ((18)) often brings misidentification into the PINN analysis. Another similarity between the two equations is that the modified RLW equation (we omit the term *modified* in the following) also has the four conserved quantities, albeit with somewhat different forms

$$\bar{I}_1 := \int \bar{i}_1(y) dy = \int u dx dy, \quad \bar{i}_1(y) := \int u dx, \quad (24)$$

$$\bar{I}_2 := \int [(\nabla u)^2 + u^2] dx dy, \quad (25)$$

$$\bar{I}_3 := \int \left( \frac{1}{2}u^2 + \frac{1}{6}u^3 \right) dx dy, \quad (26)$$

$$\bar{I}_4 := \left[ \mathbf{r}u + \mathbf{e}_x \frac{1}{2} \int_{t_0}^t (\nabla u)^2 dt' \right] dx dy - t \mathbf{e}_x \int \left\{ u + \frac{1}{2} [u^2 + (\nabla u)^2] \right\} dx dy. \quad (27)$$

The energy conservation is applied in  $\bar{I}_2$ , not the third quantity  $I_3$  like the ZK equation. The stability discussions of the RLW-type equation have been given in [73], and also [65].

### III. PRELIMINARY ANALYSIS

The PINN's deep learning method is the most effective at solving initial-boundary problems (forward problems) and reconstructing equations (inverse problems), as it can find the governing equation from given data. The following introduces the PINN method of solving data-driven vortex solutions of the non-linear quasi-integrable (2 + 1) dimensional differential equations. Throughout

analysis in the present paper, VS code is employed as the Integrated Development Environment for Python 3.11.9, and Tensorflow 2.18.0 for building PINNs. For the optimization, SciPy 1.15.1 uses the L-BFGS-B. The computation is performed on a 64-bit Windows system with an Intel(R) Core(TM)i9-14900KF CPU(3.2GHz) and NVIDIA GeForce RTX 4090 GPUs.

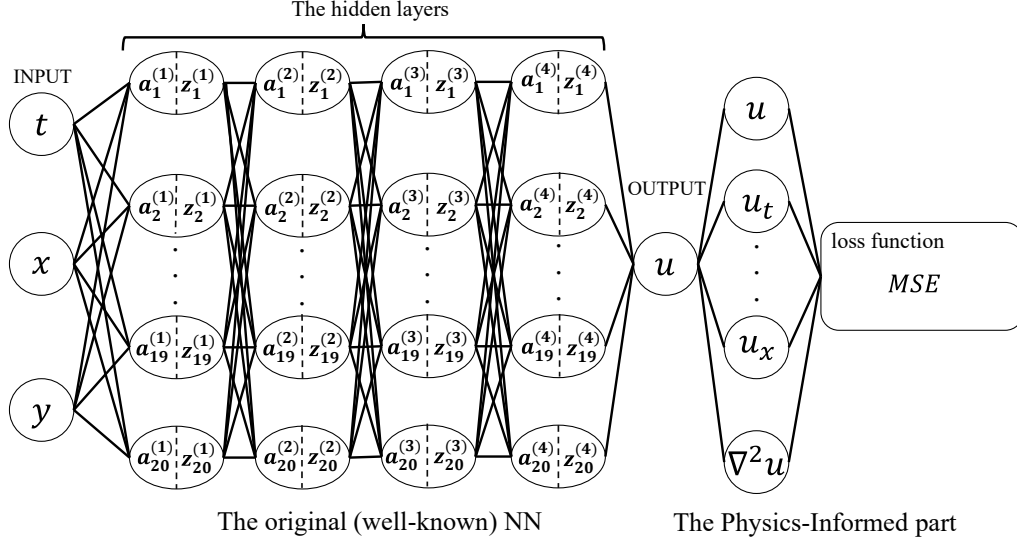


FIG. 1. The PINNs: In the first part, we first calculate the weight sum,  $a_m^{(n)} = \sum_{i=1}^{20} \{w_{im}^{(n)} z_i^{(n-1)} + b_m^{(n)}\}$  where  $(w_{lk}^{(j)}, b_k^{(j)})$  are the weighted parameters. Second, we use  $\tanh x$  as the activation function. Finally, the output is obtained through the hidden layers. After that, in the second part, we calculate the derivatives and construct a loss function.

### A. The PINNs for the (2+1)dimensional quasi-integrable systems

The method consists of two segments of the networks (see figure 1). The first is the well-known neural network's part, which is constructed with 4 hidden layers and 20 nodes for each layer to get the output  $u$  from the inputs, and time-spatial coordinates  $(x, y, t)$ . However, the output of this network has no physical meaning. In the second segment, the output derivatives and a loss function for network optimization are estimated.

The PINNs can be applied to both forward and inverse problems. The forward analysis is that one can solve a governing equation and find the solutions without ample computational resources

or sophisticated numerical algorithms. Let us consider the PDEs

$$\text{ZK eq.: } \mathcal{F}_{\text{ZK}} := u_t + \mathcal{N}_{\text{ZK}}(u, u_x, u_{xxx}, u_{xyy}) = 0, \quad (28)$$

$$\text{RLW eq.: } \mathcal{F}_{\text{RLW}} := u_t + \mathcal{N}_{\text{RLW}}(u, u_x, u_{txx}, u_{tyy}) = 0, \quad (29)$$

where  $\mathcal{N}_{\text{ZK}}$ ,  $\mathcal{N}_{\text{RLW}}$  are non-linear functions which are defined by

$$\mathcal{N}_{\text{ZK}}(u, u_x, u_{xxx}, u_{xyy}) := 2uu_x + (\nabla^2 u)_x, \quad (30)$$

$$\mathcal{N}_{\text{RLW}}(u, u_x, u_{txx}, u_{tyy}) := 2uu_x + (\nabla^2 u)_t, \quad (31)$$

respectively. For simplicity, we have removed the term  $u_x$  from the RLW equation. Although Eq.(29) is not equivalent to the RLW equation in a strict sense, as the equation without the term  $u_x$  also reduces to the normalized equation (23), a numerical traveling-wave solution still exists. We focus on the vortex solutions moving to the positive  $x$  direction of these equations. We define the rectangular mesh space

$$\begin{aligned} x &\in [-L_x, L_x], N_x \text{th grid points}; & y &\in [-L_y, L_y], N_y \text{th grid points}, \\ t &\in [T_0, T_1]. \end{aligned} \quad (32)$$

For optimization of the networks, the mean-squared error:  $MSE$  is implemented as the loss function to measure the discrepancy between the predicted and the correct values, which can be chosen such that

$$MSE = \frac{1}{N_u} \sum_{i=1}^{N_u} |u_{\text{pred}}^0(x^i, y^i, 0) - u_{\text{correct}}^0(x^i, y^i, 0)|^2 + \frac{1}{N_F} \sum_{i=1}^{N_F} |\mathcal{F}(x^i, y^i, t^i)|^2 + \frac{1}{N_b} \sum_{N_b} |\text{BC}|^2, \quad (33)$$

where  $u_{\text{pred}}^0$  is the predicted initial profile,  $u_{\text{correct}}^0$  is the correct initial profile,  $\{x^i, y^i, 0\}_{i=1}^{N_u}$  is the set of  $N_u$ th random residual points, and  $\{x^i, y^i, t^i\}_{i=1}^{N_F}$  is the  $N_F$ th random points for the PINNs  $\mathcal{F}(x, y, t)_{\text{ZK}}$  or  $\mathcal{F}(x, y, t)_{\text{RLW}}$ . Finally, BC represents the mean-squared error caused by the boundary conditions with the random  $N_b$ th points. Here, the doubly periodic boundary condition is employed so that

$$\begin{aligned} \sum_{N_b} |\text{BC}|^2 &= \sum_{i=1}^{N_{b,x}} |u_{\text{pred}}(x^i, L_y, t^i) - u_{\text{pred}}(x^i, -L_y, t^i)|^2 \\ &\quad + \sum_{j=1}^{N_{b,y}} |u_{\text{pred}}(L_x, y^j, t^j) - u_{\text{pred}}(-L_x, y^j, t^j)|^2, \end{aligned} \quad (34)$$

where  $N_b \equiv N_{b,x} + N_{b,y}$ . For optimizing the loss function, we employ the L-BFGS-B method; one of the quasi-Newton methods that can efficiently accelerate the convergence of the  $MSE$ . When

the  $MSE$  asymptotes to 0, the output  $u$  reaches the exact solution of the PDE. In figures 2 and 3, we present the typical solutions of the ZK equation and the RLW equation in terms of the forward analysis.

Another prominent application of PINNs is the guessing of the PDE from provided data. Now, we introduce a slightly modified PINNs

$$\text{ZK eq: } \tilde{\mathcal{F}}_{\text{ZK}} := u_t + \tilde{\mathcal{N}}_{\text{ZK}}(u, u_x, u_{xxx}, u_{xyy}, \boldsymbol{\lambda}) = 0, \quad (35)$$

$$\text{RLW eq: } \tilde{\mathcal{F}}_{\text{RLW}} := u_t + \tilde{\mathcal{N}}_{\text{RLW}}(u, u_x, u_{txx}, u_{tyy}, \boldsymbol{\lambda}) = 0, \quad (36)$$

where the unknown parameters  $\boldsymbol{\lambda}$  is implemented in the equations. For the inverse analysis, we employ the different  $MSE$  from (33),(34)

$$MSE = \frac{1}{N_u} \sum_{i=1}^{N_u} |u_{\text{pred}}(x^i, y^i, t^i) - u_{\text{correct}}(x^i, y^i, t^i)|^2 + \frac{1}{N_F} \sum_{i=1}^{N_F} |\tilde{\mathcal{F}}(x^i, y^i, t^i)|^2, \quad (37)$$

where  $u_{\text{pred}}$  is the predicted profile,  $u_{\text{correct}}$  is the correct profile including the boundary data,  $\{x^i, y^i, t^i\}_{i=1}^{N_u}$  is the set of  $N_u$ th random residual points, and  $\{x^i, y^i, t^i\}_{i=1}^{N_F}$  is the  $N_F$ th random points for the PINNs  $\tilde{\mathcal{F}}(x, y, t)_{\text{ZK}}$  or  $\tilde{\mathcal{F}}(x, y, t)_{\text{RLW}}$ . Automatically choosing the parameters of the Neural Networks  $(w_{lk}^{(j)}, b_k^{(j)})$  and also the parameters  $\boldsymbol{\lambda}$ , the networks are properly optimized. As a result, we obtain the proper  $\boldsymbol{\lambda}$  and then the idealized equations for corresponding training data.

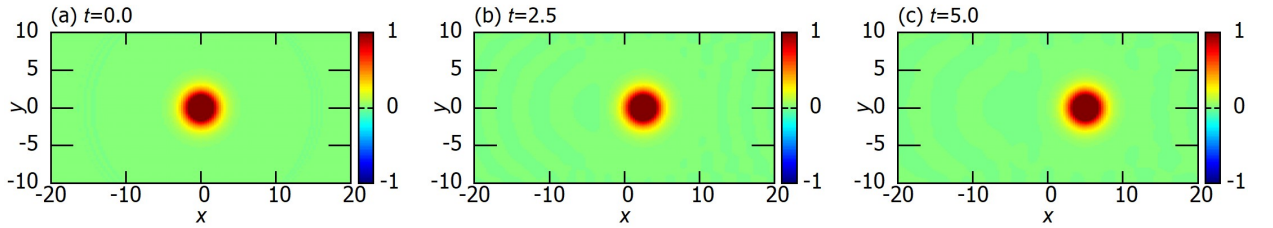


FIG. 2. The solution of the ZK equation in the forward PINN analysis.

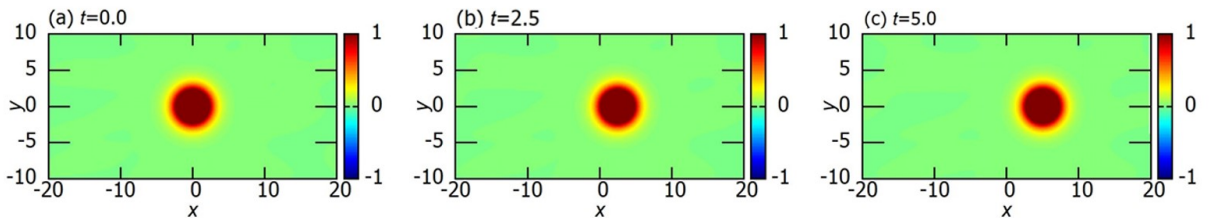


FIG. 3. The solution of the RLW equation in the forward PINN analysis.

TABLE I. The successful parameterization for the ZK equation.

	<i>PDE</i>	<i>MSE</i> ( $\times 10^{-6}$ )
Correct equation	$u_t + 2uu_x + (\nabla^2 u)_x = 0$	–
Identified (1)	$u_t + 2.046uu_x + 1.0048 (\nabla^2 u)_x = 0$	4.4
Identified (2)	$u_t + 2.011uu_x + 1.0033 (\nabla^2 u)_x = 0$	4.6

TABLE II. The successful parameterization for the RLW equation.

	<i>PDE</i>	<i>MSE</i> ( $\times 10^{-6}$ )
Correct equation	$u_t + uu_x - (\nabla^2 u)_t = 0$	–
Identified (1)	$u_t + 0.9999uu_x - 0.9996 (\nabla^2 u)_t = 0$	1.3
Identified (2)	$u_t + 0.9989uu_x - 0.9981 (\nabla^2 u)_t = 0$	1.4

### B. Successful analyses for the ZK equation and the RLW equation

As a demonstration, we employ the PINNs to solve evolution equations and the solutions found in the profile  $u$ . We define  $\tilde{\mathcal{N}}$  for the inverse analysis for the ZK equation, using two unknown constants  $\lambda_0, \lambda_1$

$$\tilde{\mathcal{N}}_{\text{ZK}}(u, u_x, u_{xxx}, u_{xyy}; \lambda_0, \lambda_1) := \lambda_0 uu_x + \lambda_1 (\nabla^2 u)_x. \quad (38)$$

We investigate the inverse analysis of the PINNs for finding the parameter values  $(\lambda_0, \lambda_1)$  using the training data derived from the forward analysis. In the PINN analysis, the numerical uncertainty is an inevitable consequence of training data sampling. We establish the correctness of our research in this paper by using the prescription of doing double identification for the same training data. In Table I, we present the result of the inverse analysis for the Zakharov-Kuznetsov equation. One can see that the PINN method reproduces the governing equation from the training data. For the RLW equation, the PINN  $\tilde{\mathcal{N}}$  is defined as

$$\tilde{\mathcal{N}}_{\text{RLW}}(u, u_x, u_{txx}, u_{tyy}, \lambda_0, \lambda_1) := 2\lambda_0 uu_x + \lambda_1 (\nabla^2 u)_t. \quad (39)$$

In the following, we shall omit the term  $u_x$  in the equation for simplicity. The result of the PINN inverse analysis is presented in Table II.

The PINN functions  $\tilde{\mathcal{N}}_{\text{ZK}}$  (38),  $\tilde{\mathcal{N}}_{\text{RLW}}$  (39) considered here are completely the same as the function of the forward analysis  $\mathcal{N}_{\text{ZK}}$  (30),  $\mathcal{N}_{\text{RLW}}$  (31), respectively making the PINN analysis successful, as shown here. Such excellent predictive power is often lost when we try to introduce

TABLE III. The misidentification for the ZK equation.

	PDE	MSE ( $\times 10^{-6}$ )
Correct equation	$u_t + 2uu_x + 0.0 (\nabla^2 u)_t + (\nabla^2 u)_x = 0$	—
Identified $c = 2(1)$	$u_t + 2.0011uu_x - 0.4017 (\nabla^2 u)_t + 0.2019 (\nabla^2 u)_x = 0$	3.8
Identified $c = 2(2)$	$u_t + 2.0015uu_x - 0.4796 (\nabla^2 u)_t + 0.0116 (\nabla^2 u)_x = 0$	4.0
Identified $c = 1(3)$	$u_t + 2.0048uu_x - 0.5190 (\nabla^2 u)_t + 0.5311 (\nabla^2 u)_x = 0$	4.1
Identified $c = 1(4)$	$u_t + 2.0452uu_x - 0.61035 (\nabla^2 u)_t + 0.4358 (\nabla^2 u)_x = 0$	5.2

a more general variant of the (38) for the inverse analysis, *i.e.*, to incorporate more complex nonlinear terms that do not exist in the original equations. The next subsection focuses on the misidentification between traveling wave solutions of the ZK equation and the RLW equation.

TABLE IV. The misidentification for the RLW equation.

	PDE	MSE ( $\times 10^{-6}$ )
Correct equation	$u_t + uu_x - (\nabla^2 u)_t + 0.0 (\nabla^2 u)_x = 0$	—
Identified $c = 2(1)$	$u_t + 0.9997uu_x - 2.0549 (\nabla^2 u)_t - 2.1105 (\nabla^2 u)_x = 0$	5.2
Identified $c = 2(2)$	$u_t + 0.9997uu_x - 1.0784 (\nabla^2 u)_t - 0.1579 (\nabla^2 u)_x = 0$	4.8
Identified $c = 1(3)$	$u_t + 0.9998uu_x - 0.8330 (\nabla^2 u)_t + 0.1666 (\nabla^2 u)_x = 0$	3.8
Identified $c = 1(4)$	$u_t + 0.9988uu_x - 0.9952 (\nabla^2 u)_t + 0.0030 (\nabla^2 u)_x = 0$	5.9

### C. The misidentification for the ZK equation and the RLW equation

We consider the following equation

$$u_t + \lambda_0 uu_x + \lambda_1 (\nabla^2 u)_t + \lambda_2 (\nabla^2 u)_x = 0. \quad (40)$$

When we choose  $(\lambda_0, \lambda_1, \lambda_2) = (2.0, 0.0, 1.0)$ , (40) becomes the ZK equation, and for  $(\lambda_0, \lambda_1, \lambda_2) = (1.0, -1.0, 0.0)$ , it reduces to the RLW equation. We study the inverse analysis both for the 1-soliton data of the ZK and the RLW equations. The PINN fails to distinguish the equations: so-called *misidentification*. We verify the inverse analysis that for the data obtained (40) leads to the ZK equation for  $(\lambda_0, \lambda_1, \lambda_2) = (2.0, 0.0, 1.0)$  and to the RLW equation for  $(\lambda_0, \lambda_1, \lambda_2) = (1.0, -1.0, 0.0)$ . As mentioned in Sec.II, the PINNs cannot distinguish these equations because they possess essentially the same traveling-wave solution  $u(x, y, t) = U(x - ct, y)$ . In Table III, we present the result of the identification of the ZK equation with the training data of the ZK vortex solution. Also, Table IV shows the identification of the RLW equation with the training data of the RLW vortex. Both identifications are completely failed.

In the following, we briefly look more closely at the origin of the stuck. Plugging the traveling-wave solution into (40), we obtain

$$-cU + \frac{\lambda_0}{2}U^2 + (\lambda_2 - c\lambda_1)\nabla^2U = 0. \quad (41)$$

If (41) comes from the ZK equation (9), the coefficients should be

$$\lambda_0 = 2.0, \quad \lambda_2 - c\lambda_1 = 1.0, \quad (42)$$

while from the RLW equation (17) with  $u_x = 0$ , it is

$$\lambda_0 = 1.0, \quad \lambda_2 - c\lambda_1 = c. \quad (43)$$

Consequently,  $\lambda_1$  and  $\lambda_2$  cannot be uniquely determined. The reason for the problem is straightforward: Since the  $t$  derivative and the  $x$  derivative for the traveling waves are convertible with one another, misinterpretation of the equation inevitably would arise in the PINN analysis. If one wishes to use the PINNs efficiently, such coincidence must be suitably broken.

#### D. The conservative PINNs: The conservation constrained deep learning

Including the conserved quantities of the ZK equation (13)-(16) and the RLW equation (24)-(27) into the  $MSE$  could potentially improve the accuracy of the guessing original equations. Here, we employ the second conserved quantity of the ZK equation

$$I_2(t) = \int \frac{u^2}{2} dx dy, \quad (44)$$

which is not the conserved quantity of the RLW equation because

$$\frac{dI_2(t)}{dt} = \int (u_x u_{xt} + u_y u_{yt}) dx dy \quad (45)$$

is not zero when we use (17) into the righthand side of (45).

We define the cPINNs: the conserved PINN algorithm which is realized by the following  $MSE$

$$MSE := \mathcal{E} + C(\mathcal{E}) \sum_{j=1}^{N_c} |I_2^{\text{pred}}(t^j) - I_2^{\text{correct}}|^2, \quad (46)$$

where the  $\mathcal{E}$  is identical to the standard  $MSE$  that was previously introduced for the forward problem (33)

$$\mathcal{E} = \frac{1}{N_u} \sum_{i=1}^{N_u} |u_{\text{pred}}^0(x^i, y^i, 0) - u_{\text{correct}}^0(x^i, y^i, 0)|^2 + \frac{1}{N_F} \sum_{i=1}^{N_F} |\mathcal{F}(x^i, y^i, t^i)|^2 + \frac{1}{N_b} \sum_{N_b} |\text{BC}|^2, \quad (47)$$

and for the inverse problem (37)

$$\mathcal{E} = \frac{1}{N_u} \sum_{i=1}^{N_u} |u_{\text{pred}}(x^i, y^i, t^i) - u_{\text{correct}}(x^i, y^i, 0)|^2 + \frac{1}{N_F} \sum_{i=1}^{N_F} |\tilde{\mathcal{F}}(x^i, y^i, t^i)|^2. \quad (48)$$

The  $N_c$  is the number of the reference time for evaluating the conserved quantity  $I_2^{\text{pred}}(t^j)$ ; here, we evaluate the integration at  $t^j = 0.0, 1.0, 2.0, 3.0, 4.0$  (i.e.,  $N_c = 5$ ) using the standard Simpson's method<sup>3</sup>.  $I_2^{\text{correct}}$  is the correct data of the conservation quantity, which is calculated by integrating  $u_{\text{correct}}(x^i, y^i, 0)$ . Since the numerical integrals of the conserved quantity diverge from the true values for non-converged solutions, which leads the undesirable loss behavior, the basic idea of the cPINNs is that the  $\mathcal{E}$  is trained first before the conservation law is considered. Now we discuss the dependence of the selection of the weight function  $C(\mathcal{E})$  on the effectiveness of our study. The weight function  $C(\mathcal{E})$  is defined in terms of a parameter  $\gamma$  and a critical value of  $\mathcal{E}_{\text{crit}}$ , such that

$$C(\mathcal{E}) = \begin{cases} f(\mathcal{E}_{\text{crit}}) & \mathcal{E} > \mathcal{E}_{\text{crit}} \\ f(\mathcal{E}) & \mathcal{E} \leq \mathcal{E}_{\text{crit}}, \end{cases} \quad (49)$$

where  $f$  is an analytic function realizing the better resolution of PINNs. In the present paper, we show the results using the following three types of  $f(\mathcal{E})$

$$f(\mathcal{E}) = \begin{cases} \exp(-\gamma\mathcal{E}) & \text{:exponential} \\ \frac{2}{1 + \exp(\gamma\mathcal{E})} & \text{:sigmoid} \\ \log(1 + \exp(-\gamma\mathcal{E})) & \text{:softplus.} \end{cases} \quad (50)$$

We choose the parameters as  $\gamma = 5.0 \times 10^4$ ,  $\mathcal{E}_{\text{crit}} = 1.0 \times 10^{-3}$  of  $C(\mathcal{E})$  by trial and error, realizing the lowest value of  $MSEs$ . We plot the behavior of  $C(\mathcal{E})$  in Fig.4. We demonstrate the identification of the ZK equation with three types of the weight functions (50). One can easily find that the results do not significantly depend on the choice of the weight functions shown in Table V. In the following, we only employ the exponential function and change the value of the coupling parameter  $\gamma$ .

---

<sup>3</sup> More sophisticated formula such as the Gauss quadrature is available but no notable difference occurs in the final result.

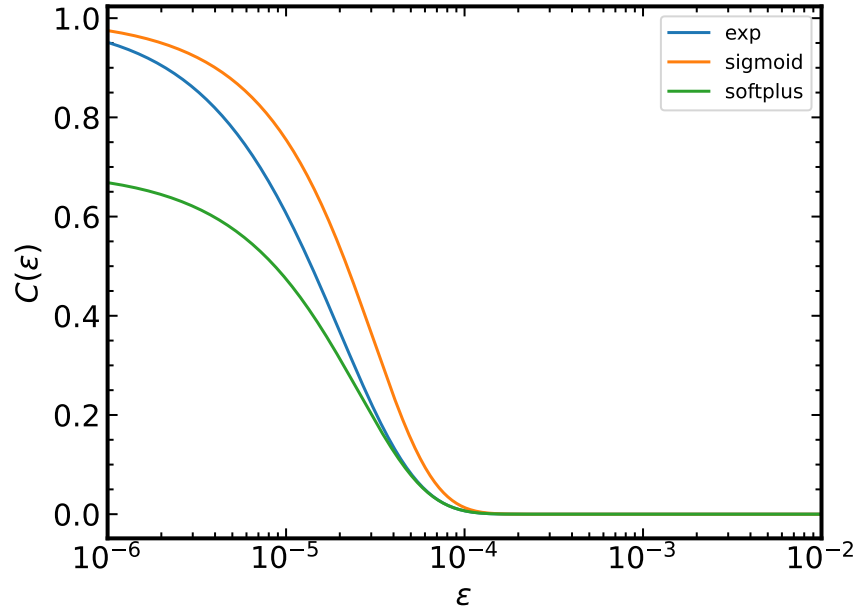


FIG. 4. The behavior of  $C(\mathcal{E})$  defined by (49),(50) for  $\gamma = 5.0 \times 10^4$  and  $\mathcal{E}_{\text{crit}} = 1.0 \times 10^{-3}$ .

TABLE V. The identification of the ZK equation in the  $MSE$  (46). The parameter of  $f(\mathcal{E})$  is fixed as  $\gamma = 5.0 \times 10^4$ .

	$f(\mathcal{E})$	$PDE$	$MSE (\times 10^{-6})$
Correct equation	-	$u_t + 2uu_x + (\nabla^2 u)_x = 0$	-
Identified	exp	$u_t + 2.019uu_x + 0.5659 (\nabla^2 u)_x - 0.4524 (\nabla^2 u)_t = 0$	2.0
Identified	sigmoid	$u_t + 1.920uu_x + 0.7121 (\nabla^2 u)_x - 0.5641 (\nabla^2 u)_t = 0$	11
Identified	softplus	$u_t + 1.751uu_x + 0.3289 (\nabla^2 u)_x - 0.3316 (\nabla^2 u)_t = 0$	35

The profile of the single soliton via cPINNs is presented in Fig.5. To verify the accuracy of the cPINNs, we assess the variation from the numerical analysis:  $u_{\text{pred}} - u_{\text{correct}}$ , and the predictability of the cPINNs is much better than that of the PINN analysis as we can see in Fig.6.

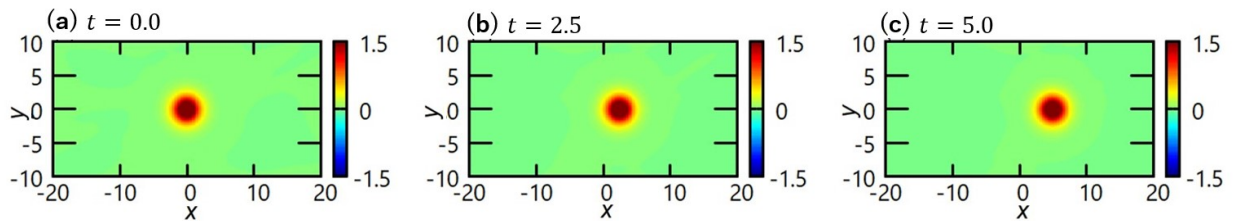


FIG. 5. single soliton profile predicted by cPINNs. the parameters for the  $C(\mathcal{E})$  are fixed as  $\gamma = 5.0 \times 10^4$ ,  $\mathcal{E}_{\text{crit}} = 1.0 \times 10^{-3}$ .

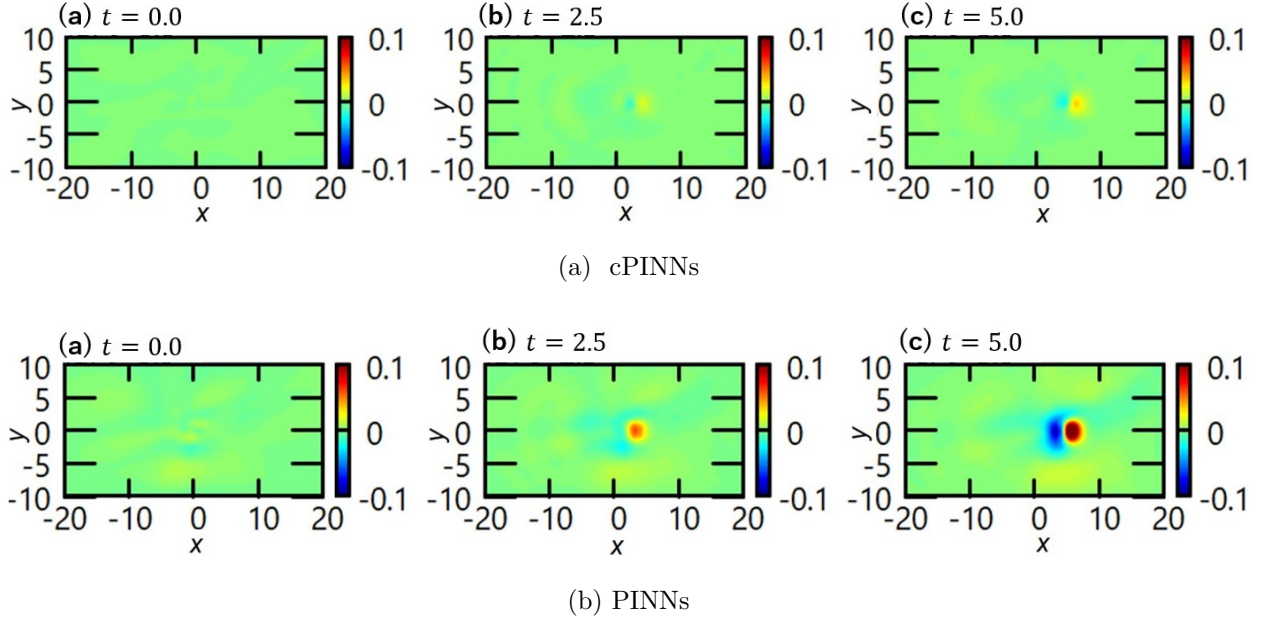


FIG. 6. The error between the predicted profile and the numerical solution:  $u_{\text{pred}} - u_{\text{correct}}$  of the (a) cPINNs, and (b) PINNs.

However, as shown in Table VI, for the predictability compare with the PINNs, cPINNs are ineffective. The main reason for the failure is that the cPINN's projected profile is more accurate than that of PINNs and the output of the cPINNs is closer to  $u_{\text{pred}}(x, y, t) \sim U(x - ct, y)$ . Unfortunately, the misidentification may be the result of our attempt to improve the predictability by considering the conserved quantities as described in this section.

TABLE VI. The identification of the ZK equation in the  $MSE$  (46) with changing the coupling parameter  $\alpha$ .

	$\gamma (\times 10^3)$	$PDE$	$MSE (\times 10^{-6})$
Correct equation	–	$u_t + 2uu_x + (\nabla^2 u)_x = 0$	–
Identified	50	$u_t + 2.019uu_x + 0.5659 (\nabla^2 u)_x - 0.4524 (\nabla^2 u)_t = 0$	2.0
Identified	10	$u_t + 2.020uu_x + 0.5648 (\nabla^2 u)_x - 0.4524 (\nabla^2 u)_t = 0$	2.0
Identified	5	$u_t + 2.020uu_x + 0.5676 (\nabla^2 u)_x - 0.4511 (\nabla^2 u)_t = 0$	2.2
Identified	1	$u_t + 0.6362uu_x + 0.0351 (\nabla^2 u)_x - 0.00913 (\nabla^2 u)_t = 0$	611

### E. The 2-soliton solution

For the next application, we consider the 2-soliton initial profile. This is no longer solution of the equation although each soliton is a traveling wave solution. We place two single solitons far

enough so that they never collide with each other. We define the initial profile

$$u(x, y, 0) = U_{c_1}(x - x_0, y) + U_{c_2}(x + x_0, y), \quad (51)$$

where  $c_1$  and  $c_2$  are the speed of each soliton, respectively. The initial profile does not possess convertibility of the  $x$  derivative and the  $t$  derivative. For the training data of the inverse analysis, we employ the segment data:  $t \in$  (a)  $[0.0, 3.3)$ , (b)  $[3.3, 6.6)$ , (c)  $[6.6, 9.9)$ , (d)  $[9.9, 13.3)$ , (e)  $[13.3, 16.6)$ , (f)  $[16.6, 19.9)$ , as plotted in Fig.7. The results of the inverse analysis are presented in Table VII. The accuracy has been certainly improved, but the *MSEs* still need to be improved. There is yet another major disadvantage in this scheme. It is now becoming evident that the PINN inverse analysis loses the resolutions when two solitons experience the collision processes, and this might happen in this instance [53]. In the following section, we will discuss the novel prescriptions for improving resolution that do not rely on the dynamics of the 2-soliton.

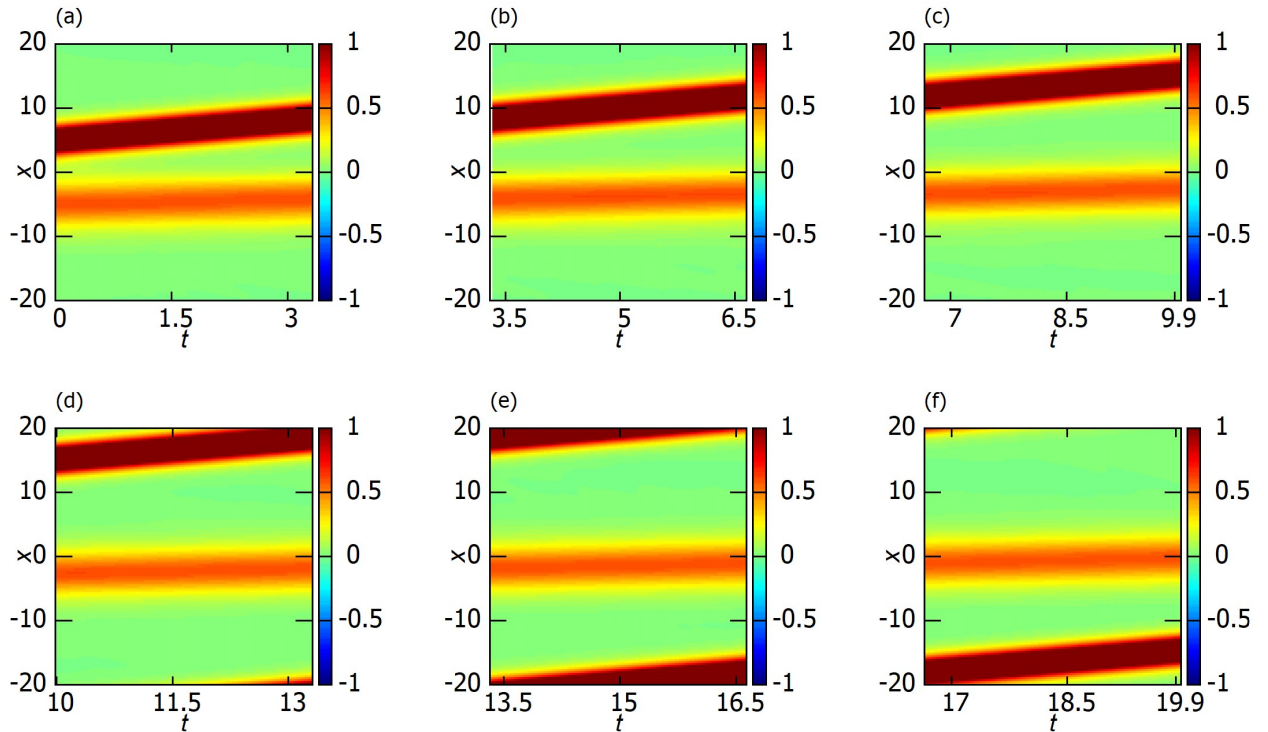


FIG. 7. 2-soliton training data of  $c_1 = 1.0, c_2 = 0.25, x_0 = 6.0$ . with the time segment of (a)  $t \in [0.0, 3.3)$ , (b)  $t \in [3.3, 6.6)$ , (c)  $t \in [6.6, 9.9)$ , (d)  $t \in [9.9, 13.3)$ , (e)  $t \in [13.3, 16.6)$ , (f)  $t \in [16.6, 19.9)$ .

TABLE VII. The identification of the ZK equation in terms of the 2-soliton with the small time segment data:  $t \in$  (a) [0.0, 3.3), (b) [3.3, 6.6), (c) [6.6, 9.9), (d) [9.9, 13.3), (e) [13.3, 16.6), (f) [16.6, 19.9).

	<i>PDE</i>	<i>MSE</i> ( $\times 10^{-6}$ )
Correct equation	$u_t + 2uu_x + 0.0 (\nabla^2 u)_t + (\nabla^2 u)_x = 0$	—
Identified (a)	$u_t + 2.056uu_x - 0.001 (\nabla^2 u)_t + 1.058 (\nabla^2 u)_x = 0$	5.0
Identified (b)	$u_t + 2.046uu_x - 0.029 (\nabla^2 u)_t + 1.020 (\nabla^2 u)_x = 0$	5.3
Identified (c)	$u_t + 2.004uu_x - 0.026 (\nabla^2 u)_t + 1.014 (\nabla^2 u)_x = 0$	6.5
Identified (d)	$u_t + 2.032uu_x - 0.039 (\nabla^2 u)_t + 0.997 (\nabla^2 u)_x = 0$	8.3
Identified (e)	$u_t + 1.991uu_x - 0.021 (\nabla^2 u)_t + 0.996 (\nabla^2 u)_x = 0$	9.8
Identified (f)	$u_t + 2.050uu_x - 0.005 (\nabla^2 u)_t + 1.060 (\nabla^2 u)_x = 0$	5.5

#### IV. DATA-DRIVEN DISCOVERY OF THE GOVERNING EQUATIONS

In this section, we would like to examine the equations predicted from the data of the single vortex with some non-trivial “twists”. It is unquestionably useful because observational data increase various noises, modulations to some degree, and other disturbances to some degree. Therefore, the attempt to derive the governing equation using PINNs from data with contamination. We give a few examples that successfully identify the governing equations.

##### A. Deformation of the initial profile

One of the reasons for the misidentification is that we employed the traveling-wave solution of the normalized equation (23) as the initial profile. A non-linear PDE often has numerous independent solutions caused by differences in the initial conditions [74], providing deeper insight into the mathematical meanings of the equation and the phenomena of our concern. If we use the data with the various initial profiles in the PINN inverse analysis, the resolution improves because this prescription would break the condition  $\frac{\partial u}{\partial x} = -c \frac{\partial u}{\partial t}$ . The Gaussian profile

$$u(x, y, 0) := 2.0 \exp \left[ -\frac{1}{\ell} (x^2 + y^2) \right] \quad (52)$$

is widely used in the analysis of several evolution equations in two spatial dimensions. It also can be an initial profile of the ZK and the RLW equations, so we numerically solve these governing equations and get the data for the inverse analysis. We present the results the for forward analysis of the ZK equation with the initial profiles (52) of the several scales  $\ell = 2.5, 5.0, 7.5$  and 10.0 in Figure 8. The results of the inverse analysis for the several data with  $\ell$  from 2.25 to 10.0 are

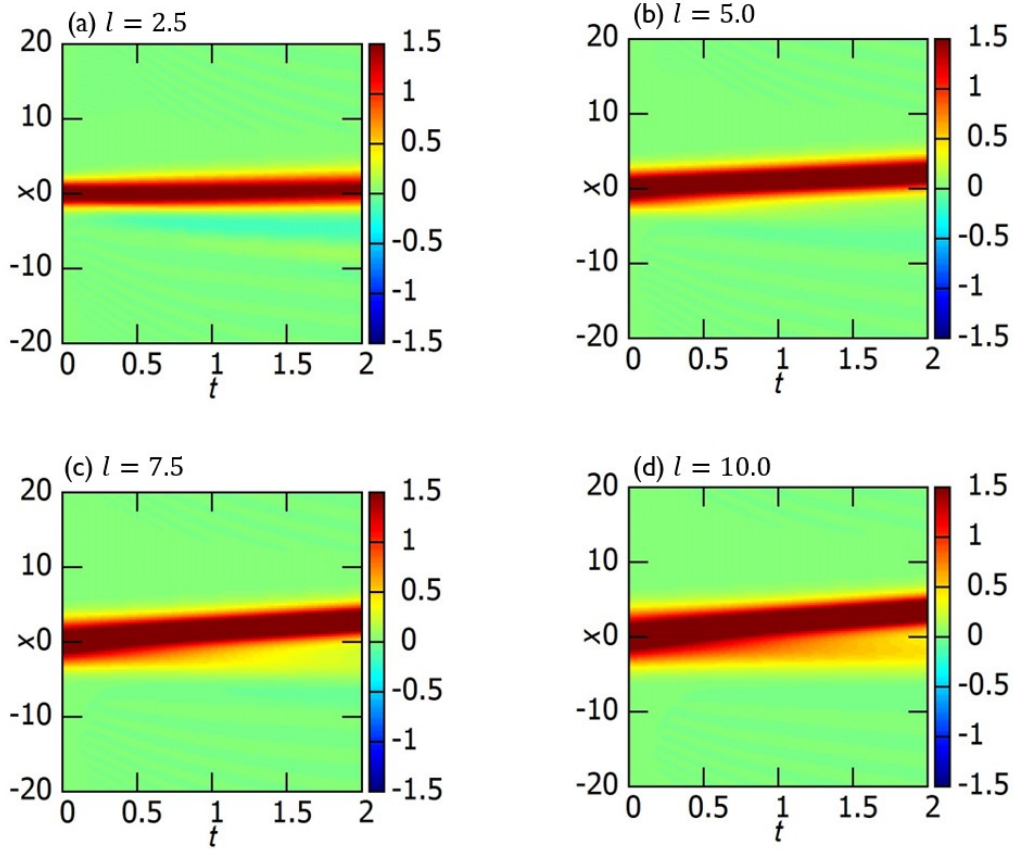


FIG. 8. The time evolution of the Gaussian profiles with  $\ell = 2.5, 5.0, 7.5,$  and  $10.0$ .

given in Table VIII. The results show that, as the  $MSE$  is not small enough ( $\sim 10^{-5}$ ), further convergence has to be attained.

TABLE VIII. The identification of the ZK equation using the data of the Gaussian initial profiles.

	$PDE$	$MSE (\times 10^{-5})$
Correct equation	$u_t + 2uu_x + 0.0 (\nabla^2 u)_t + (\nabla^2 u)_x = 0$	—
Identified $\ell = 2.25$	$u_t + 1.986uu_x - 0.0581 (\nabla^2 u)_t + 0.9797 (\nabla^2 u)_x = 0$	6.1
Identified $\ell = 2.50$	$u_t + 2.0407uu_x - 0.0569 (\nabla^2 u)_t + 1.0106 (\nabla^2 u)_x = 0$	3.7
Identified $\ell = 2.75$	$u_t + 2.0558uu_x - 0.0771 (\nabla^2 u)_t + 1.0102 (\nabla^2 u)_x = 0$	2.3
Identified $\ell = 4.75$	$u_t + 2.0624uu_x - 0.1149 (\nabla^2 u)_t + 0.94666 (\nabla^2 u)_x = 0$	3.8
Identified $\ell = 5.0$	$u_t + 2.0599uu_x - 0.14533 (\nabla^2 u)_t + 0.92023 (\nabla^2 u)_x = 0$	3.0
Identified $\ell = 5.25$	$u_t + 2.05069uu_x - 0.06841 (\nabla^2 u)_t + 0.97961 (\nabla^2 u)_x = 0$	2.4
Identified $\ell = 7.25$	$u_t + 2.0534uu_x - 0.0475 (\nabla^2 u)_t + 0.9973 (\nabla^2 u)_x = 0$	1.8
Identified $\ell = 7.50$	$u_t + 2.05035uu_x - 0.04637 (\nabla^2 u)_t + 0.9950 (\nabla^2 u)_x = 0$	1.7
Identified $\ell = 7.75$	$u_t + 2.04880uu_x - 0.052728 (\nabla^2 u)_t + 0.9840 (\nabla^2 u)_x = 0$	2.0
Identified $\ell = 10.0$	$u_t + 2.0473uu_x - 0.0369 (\nabla^2 u)_t + 0.9976 (\nabla^2 u)_x = 0$	1.3

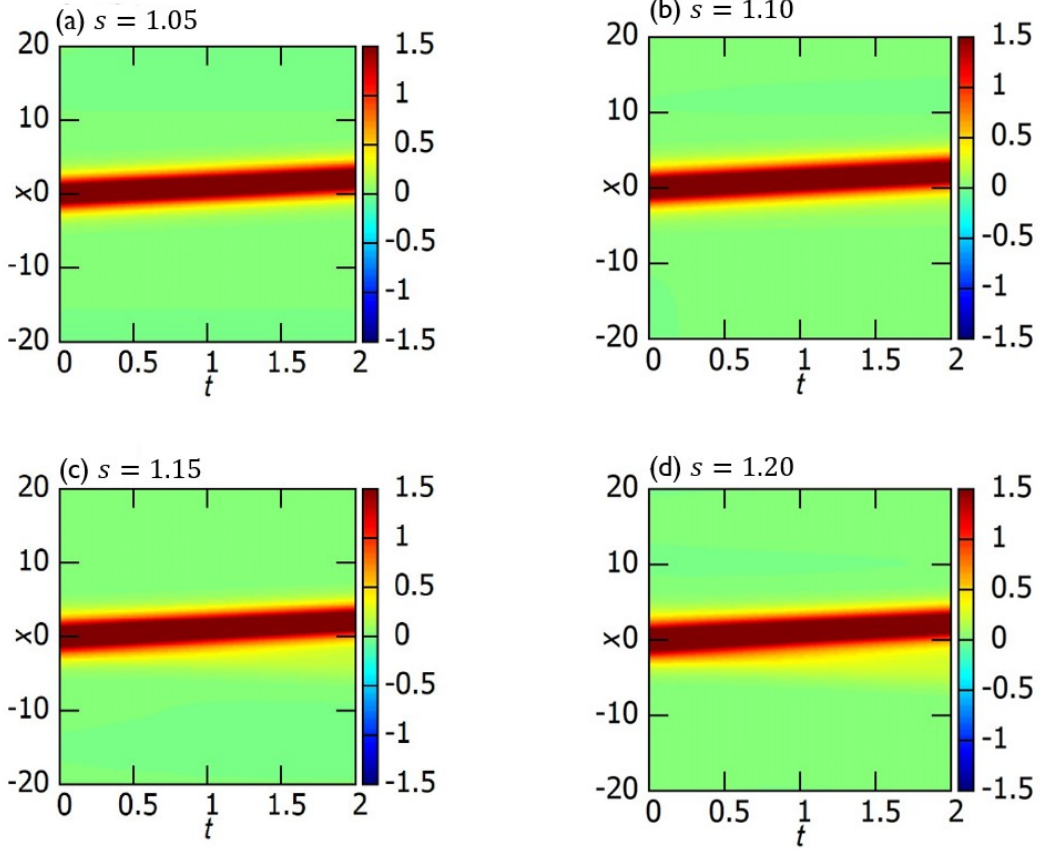


FIG. 9. The time evolution of the oval-shaped profiles with  $s = 1.05, 1.10, 1.15,$  and  $1.20$ .

Another initial profile might have more physical meaning. In geophysical flow dynamics as seen in Jupiter's GRS, the oval-shaped profile is frequently observed. Also, the ZK equation is a toy model of the intermediate geostrophic regime, which is believed to govern the GRS. We employ the following form of the initial condition

$$u(x, y, 0) := U\left(s\xi, \frac{1}{s}y\right), \quad s > 1. \quad (53)$$

Again it breaks the coincidence  $\frac{\partial u}{\partial x} = -c \frac{\partial u}{\partial t}$ , then improves the PINNs' resolution. We present the results for the forward analysis of the ZK equation with the initial profile (53) with the several deformation parameter values  $s = 1.05, 1.1, 1.15,$  and  $1.20$  in Fig. 9. The results of the inverse analysis for the several data with  $s$  from  $1.0$  to  $1.2$  are in Table IX. Apparently, the predictive power of the PINNs is certainly improved for  $s > 1.125$ . At the same time, we must admit that the current prescription has a downside that excessive deformation often contaminates the vortex later. The origin of the instability is that it inevitably violates the conservation laws. We conclude that while using deformed initial profiles is somewhat promising, but it is only if the deviation from the circular shape of the initial profile is small.

Here, it is worthwhile to address why the resolution of the PINNs has been improved. In Fig.10, we plot the velocity of the center of the vortices in the case of Gaussian and oval profiles. The blue-shaded areas indicate where the identifications of the equations fail. The speed of the vortices appears to be crucial; the identification is only successful when the velocities are outside the blue regions.

TABLE IX. The identification of the ZK equation with the data of the oval-shaped initial profiles.

	$PDE$	$MSE (\times 10^{-6})$
Correct equation	$u_t + 2uu_x + 0.0 (\nabla^2 u)_t + (\nabla^2 u)_x = 0$	—
Identified $s = 1.000$	$u_t + 1.995uu_x - 0.0581 (\nabla^2 u)_t + 0.45367 (\nabla^2 u)_x = 0$	1.5
Identified $s = 1.025$	$u_t + 2.0140uu_x - 0.5489 (\nabla^2 u)_t + 0.45300 (\nabla^2 u)_x = 0$	3.4
Identified $s = 1.050$	$u_t + 2.0241uu_x - 0.4677 (\nabla^2 u)_t + 0.53675 (\nabla^2 u)_x = 0$	6.8
Identified $s = 1.075$	$u_t + 2.02010uu_x - 0.4754 (\nabla^2 u)_t + 0.51766 (\nabla^2 u)_x = 0$	11.8
Identified $s = 1.100$	$u_t + 2.0248uu_x - 0.3649 (\nabla^2 u)_t + 0.64731 (\nabla^2 u)_x = 0$	13.6
Identified $s = 1.125$	$u_t + 1.99602uu_x - 0.07228 (\nabla^2 u)_t + 0.92303 (\nabla^2 u)_x = 0$	9.5
Identified $s = 1.150$	$u_t + 2.00005uu_x - 0.08176 (\nabla^2 u)_t + 0.91783 (\nabla^2 u)_x = 0$	10.2
Identified $s = 1.175$	$u_t + 1.9961uu_x - 0.06765 (\nabla^2 u)_t + 0.92731 (\nabla^2 u)_x = 0$	13.0
Identified $s = 1.200$	$u_t + 1.9975uu_x - 0.03614 (\nabla^2 u)_t + 0.9611 (\nabla^2 u)_x = 0$	12.8

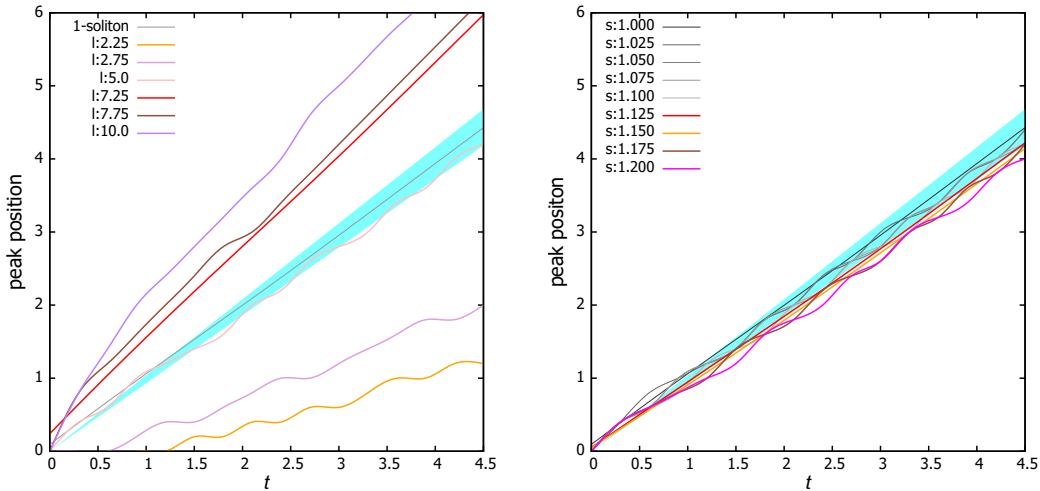


FIG. 10. The position of the center of the vortices of the Gaussian deformation (left) and the oval-shaped deformation (right). The blue-shaded areas indicate that the identification of the equations is unsuccessful, roughly the relation  $u_t \sim -u_x$  is satisfied.

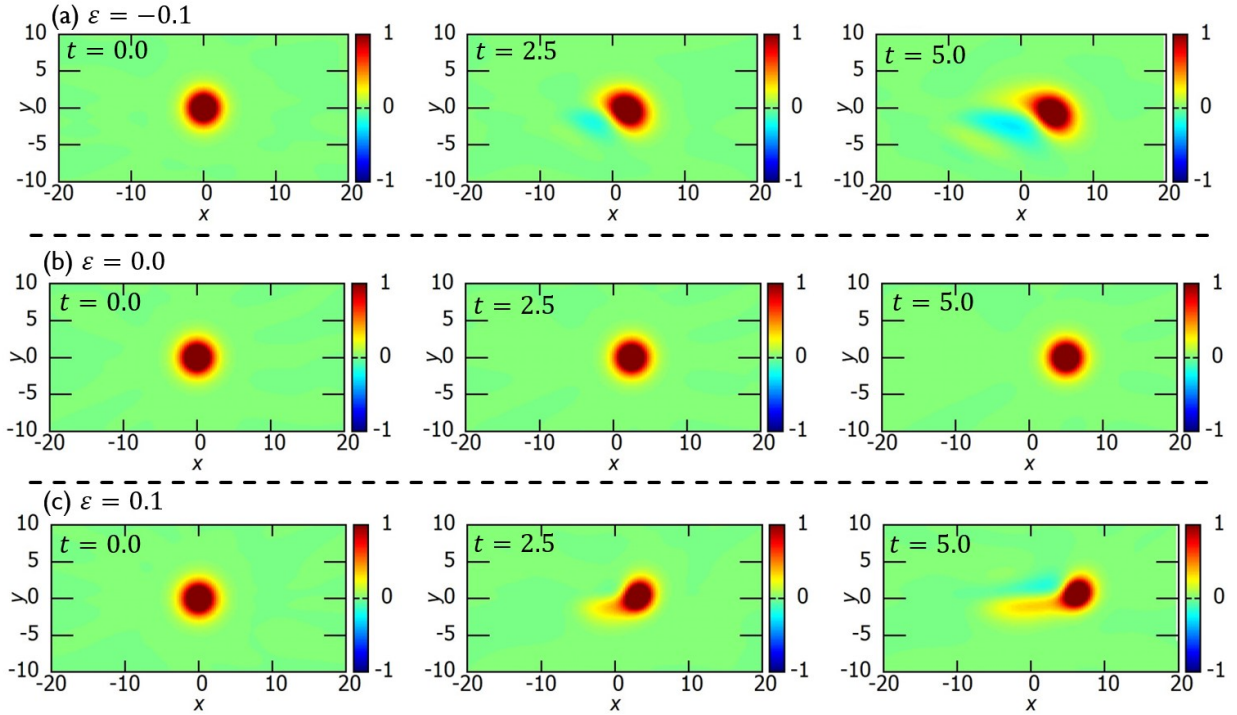


FIG. 11. The training data with constant current  $u_0 = -1.0 + \varepsilon$ , where (a):  $\varepsilon = -0.1$ ,(b):  $\varepsilon = 0.0$ ,(c):  $\varepsilon = 0.1$ .

### B. A perturbative friction via a background flow

Both the RLW and the ZK equations are governing equations of the plasma or the fluid dynamics. In fact, the former is a simplified form of the drift wave equation in plasma or the quasi-geostrophic equation describing Rossby waves in rotating fluid when we omit the Jacobian-type non-linear term from the governing equation. The latter is closely connected with the intermediate geostrophic regime of the shallow water dynamics [15]. The equation possesses the anti-cyclonic stable vortex, which is supposed to be a candidate of the GRS. For both the drift wave equation and the intermediate geostrophic equation, the existence of the shear flows is crucial for obtaining the stable, long-lived solutions [15, 17, 75].

Our goal here is to enhance the PINNs' performance by utilizing the influence of the background flow. For this purpose, we use the above intermediate geostrophic equation to find the perturbative

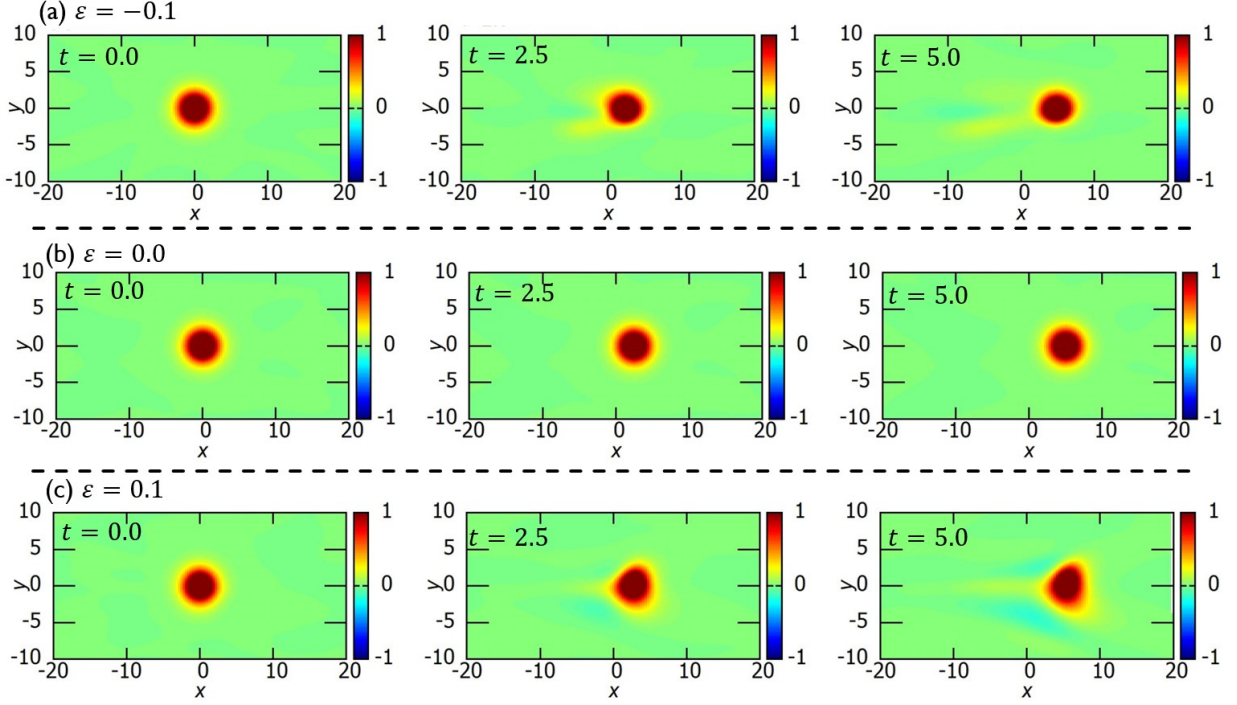


FIG. 12. The training data with  $y$ -dependent flow  $u_0 = -1.0 + \varepsilon y$ , where (a):  $\varepsilon = -0.1$ , (b):  $\varepsilon = 0.0$ , (c):  $\varepsilon = 0.1$ .

friction term. The equation for the cyclonic shear [15, 16] is

$$\frac{\partial \eta}{\partial t} + 2\eta \frac{\partial \eta}{\partial x} - \frac{\partial}{\partial x}(\nabla^2 \eta) + 2y \frac{\partial \eta}{\partial x} - 2J[\nabla^2 \eta, \eta] = 0. \quad (54)$$

The last term, the Jacobian represents the geostrophic advection of vorticity  $\nabla^2 \eta$  in the words in fluid mechanics, and we refer to it as the vector nonlinear term. The stream function  $\eta := \eta(x, y, t)$  is expanded by the shear zonal flow  $u_0(y)$  such as

$$\eta(x, y, t) = \int_0^y u_0(y') dy' + u(x, y, t), \quad (55)$$

where the field  $u(x, y, t)$  is a perturbation from the sole existence of the zonal flow. If we set  $u_0 = -1.0$  and omit the Jacobian, the equation becomes the ZK equation [17]. Setting the constant current  $u_0$  in ((55)) as

$$u_0^1 := -1.0 + \varepsilon, \quad |\varepsilon| \ll 1, \quad (56)$$

we can write down (54) in terms of  $u$  such as

$$u_t + 2uu_x + (\nabla^2 u)_x - 2J[\nabla^2 u, u] + 2\varepsilon\{yu_x - (\nabla^2 u)_x\} = 0. \quad (57)$$

After the removal of the Jacobian, the perturbative term which we use later becomes

$$\varepsilon \mathcal{N}^1(u_x, u_{xxx}, u_{xyy}) := 2\varepsilon \{yu_x - (\nabla^2 u)_x\}. \quad (58)$$

Similarly, if we consider a  $y$ -dependent shear flow and set  $u_0^2(y)$  as

$$u_0^2(y) := -1.0 + \varepsilon y, \quad |\varepsilon| \ll 1, \quad (59)$$

we find

$$\varepsilon \mathcal{N}^2(u_x, u_{xxx}, u_{xyy}) := \varepsilon \{y^2 u_x - 2y (\nabla^2 u)_x\}. \quad (60)$$

The modified ZK equation is defined as

$$\mathcal{F}_{\text{mZK}}^a = u_t + \mathcal{N}_{\text{ZK}}(u, u_x, u_{xxx}, u_{xyy}) + \varepsilon \mathcal{N}^a(u_x, u_{xxx}, u_{xyy}) = 0, \quad a = 1, 2. \quad (61)$$

Note that the equation of  $\mathcal{F}_{\text{mZK}}^1$  possesses four conserved quantities, where the first two  $I_1, I_2$  is completely same as those of the ZK equation while the other conserved quantities  $I_3, I_4$  are slightly modified from (15) and (16) to

$$I_3' := \int \left[ (\nabla u)^2 - \frac{1}{1-2\varepsilon} \frac{1}{3} u^3 - \frac{\varepsilon}{1-2\varepsilon} y u^2 \right] dx dy, \quad (62)$$

$$I_4' := \int \mathbf{r} u dx dy - \mathbf{t} e_x \int (u^2 + 2\varepsilon y u) dx dy. \quad (63)$$

The  $I_3'$  corresponds to the total energy in  $\mathcal{F}_{\text{mZK}}^1$ . It is simply obtained on multiplying  $\nabla^2 u$  by the equation and using the doubly periodic boundary condition to integrate it on the whole area. It comprises the kinetic energy:  $(\nabla u)^2$ , a potential energy:  $u^3$ , and also a twisting term:  $y u^2$ . Note that the  $|\varepsilon|$  is small, so the denominators in (62) never become zero. The solutions of the equation  $\mathcal{F}_{\text{mZK}}^1$  are stable for the time evolution because the energy is conserved. On the other hand, the energy of the  $\mathcal{F}_{\text{mZK}}^2$  is not conserved, and the solutions tend to be unstable. We present the results of the forward analysis of  $\mathcal{F}_{\text{mZK}}^1$  in Fig.11 and  $\mathcal{F}_{\text{mZK}}^2$  in Fig.12. Here, we plot the solutions with the strength of the perturbative terms  $\varepsilon = -1.0, 0.0$ , and  $1.0$ .

The inverse analysis is operated with

$$\tilde{\mathcal{F}} = u_t + \tilde{\mathcal{N}}(u, u_x, u_{txx}, u_{tyy}, u_{xxx}, u_{xyy}, \boldsymbol{\lambda}) + \varepsilon \mathcal{N}_1(u_x, u_{xxx}, u_{xyy}) = 0, \quad (64)$$

$$\tilde{\mathcal{N}}(u, u_x, u_{txx}, u_{tyy}, u_{xxx}, u_{xyy}, \lambda_0, \lambda_1, \lambda_2) := \lambda_0 u u_x + \lambda_1 (\nabla^2 u)_t + \lambda_2 (\nabla^2 u)_x. \quad (65)$$

The results are shown in Fig.13. Using the results of the forward analysis to obtain the solution of (61), we compute the root mean-squared error of the model parameters defined as

$$RMSE := \sqrt{\frac{\sum_{i=0}^2 |\lambda_i^{\text{pred}} - \lambda_i^{\text{correct}}|^2}{3}}. \quad (66)$$

We find that significant improvement in the resolution of the predictability is realized in the case considering the constant current with the certain perturbation. However, case of the  $y$ -dependent current, which changes the original ZK equation into a non-conservative equation, cannot improve the predictability of the PINNs. As a result, we conclude that PINN predictability can be increased with a small perturbation that keeps the conservation laws.

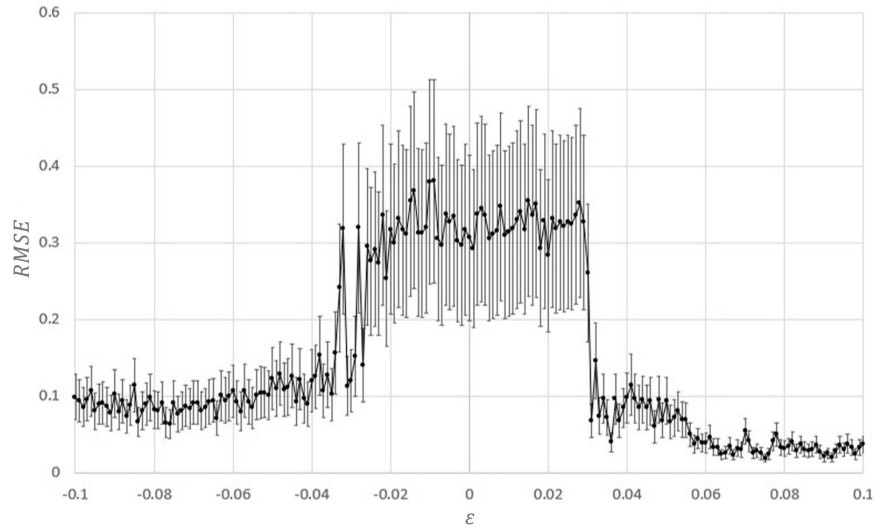
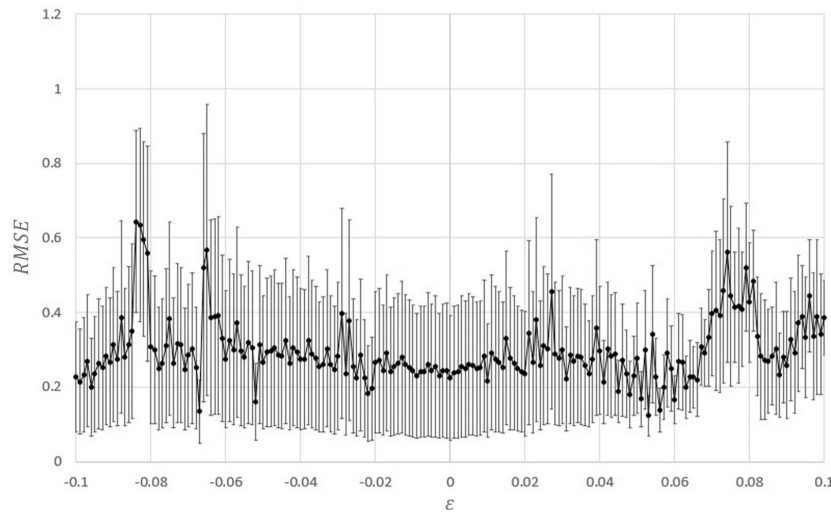
(a)  $u_0 := -1.0 + \varepsilon$ (b)  $u_0 := -1.0 + \varepsilon y$ 

FIG. 13. Relation between the accuracy of the identification and strength of the perturbative term induced to the ZK equation  $\varepsilon$ . The root mean-squared error:  $RMSE = \sqrt{\frac{\sum_{i=0}^2 |\lambda_i^{\text{pred}} - \lambda_i^{\text{correct}}|^2}{3}}$  is: (a) suppressed for  $\varepsilon \gtrsim 0.05$  in case of the constant current, (b) ineffective suppression of the  $RMSE$  in the case of the  $y$ -dependent current. In this calculation, the inverse problem analysis is performed five times for the configurations obtained at each  $\varepsilon$ . The average of the RMSEs is drawn by the solid black line, and the standard uncertainty for each is represented by the gray line.

TABLE X. The identification of the ZK equation using the vortex data with constant current  $\varepsilon = 0.001$ .

	<i>PDE</i>
Correct equation	$u_t + 2uu_x + (\nabla^2 u)_x = 0$
Identified(1)	$u_t + 1.996uu_x + 0.5476 (\nabla^2 u)_x - 0.4503 (\nabla^2 u)_t = 0$
Identified(2)	$u_t + 1.993uu_x + 0.7105 (\nabla^2 u)_x - 0.2839 (\nabla^2 u)_t = 0$
Identified(3)	$u_t + 1.997uu_x + 0.5657 (\nabla^2 u)_x - 0.4326 (\nabla^2 u)_t = 0$
Identified(4)	$u_t + 1.999uu_x + 0.3839 (\nabla^2 u)_x - 0.6170 (\nabla^2 u)_t = 0$
Identified(5)	$u_t + 1.996uu_x + 0.5573 (\nabla^2 u)_x - 0.4433 (\nabla^2 u)_t = 0$
Standard uncertainty of <i>RMSE</i>	0.108

TABLE XI. The identification of the ZK equation using the vortex data with constant current  $\varepsilon = 0.04$ .

	<i>PDE</i>
Correct equation	$u_t + 2uu_x + (\nabla^2 u)_x = 0$
Identified(1)	$u_t + 2.016uu_x + 1.136 (\nabla^2 u)_x + 0.1535 (\nabla^2 u)_t = 0$
Identified(2)	$u_t + 2.023uu_x + 1.143 (\nabla^2 u)_x + 0.1646 (\nabla^2 u)_t = 0$
Identified(3)	$u_t + 2.009uu_x + 1.132 (\nabla^2 u)_x + 0.1452 (\nabla^2 u)_t = 0$
Identified(4)	$u_t + 2.001uu_x + 1.124 (\nabla^2 u)_x + 0.1387 (\nabla^2 u)_t = 0$
Identified(5)	$u_t + 2.019uu_x + 1.125 (\nabla^2 u)_x + 0.1233 (\nabla^2 u)_t = 0$
Standard uncertainty of <i>RMSE</i>	<b>0.031</b>

TABLE XII. The identification of the ZK equation using the vortex data with constant current  $\varepsilon = 0.1$ .

	<i>PDE</i>
Correct equation	$u_t + 2uu_x + (\nabla^2 u)_x = 0$
Identified(1)	$u_t + 2.014uu_x + 1.040 (\nabla^2 u)_x + 0.035 (\nabla^2 u)_t = 0$
Identified(2)	$u_t + 2.091uu_x + 1.011 (\nabla^2 u)_x + 0.026 (\nabla^2 u)_t = 0$
Identified(3)	$u_t + 2.013uu_x + 1.013 (\nabla^2 u)_x + 0.018 (\nabla^2 u)_t = 0$
Identified(4)	$u_t + 2.002uu_x + 1.021 (\nabla^2 u)_x + 0.027 (\nabla^2 u)_t = 0$
Identified(5)	$u_t + 2.012uu_x + 1.025 (\nabla^2 u)_x + 0.022 (\nabla^2 u)_t = 0$
Standard uncertainty of <i>RMSE</i>	<b>0.009</b>

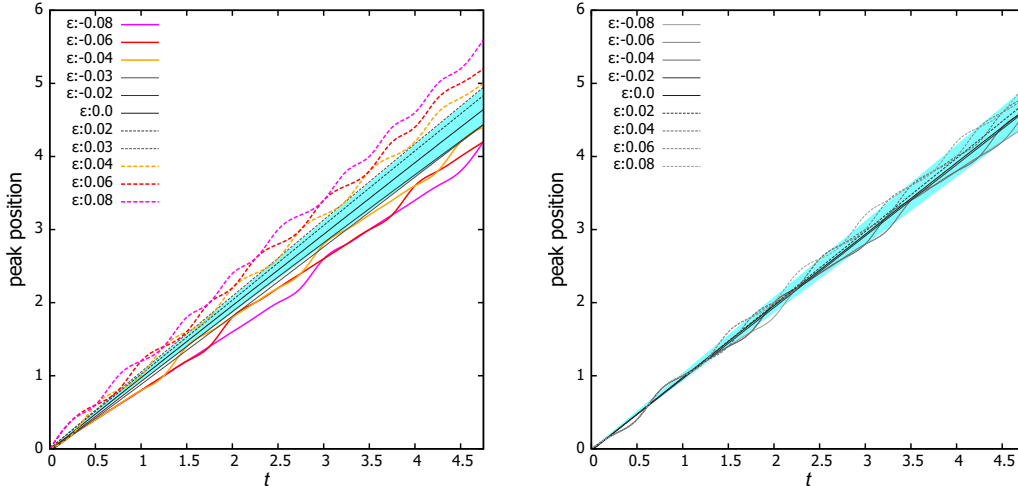


FIG. 14. The position of the center of the vortices of the constant current (left) and the  $y$ -dependent current (right). The blue-shaded areas indicate that the identification of the equations is unsuccessful, roughly the relation  $u_t \sim -u_x$  is satisfied.

To quantitatively evaluate the improvement in resolution of the PINNs, we performed the inverse problem analysis five times using the vortex data corresponding to three different values of  $\epsilon$  to compute  $RMSE$ . The standard error of the  $RMSE$  represents the degree of misidentification: In FIG.13, the error-bars indicate the uncertainty in the equation determination. These results suggest that the vortex data considering constant current with  $|\epsilon| \gtrsim 0.04$  produce several times smaller errors in the inverse problem than the other data. Fig.14 again shows the velocities of the center of the vortices with the perturbations. One can directly see that in the case of the  $y$ -dependent current, the solutions always stick into the blue-shaded area, and then, the resolution fails to recover. Finally, we show more explicitly the behavior depending on the coefficients of the constant current with some values of  $\epsilon$ . In Tables X - XII, we present the results of the identification for the ZK equation and the uncertainty of the identification.

## V. SUMMARY

In this paper, we investigated the PINNs to analyze the quasi-integrable non-linear differential equations: the Zakharov-Kuznetsov equation and the regularized long-wave equation. These equations share some common structures for their traveling-wave solutions, and then the PINNs fail to identify them from the data. The identifications are improved by using the various beginning profiles, such as the Gaussian and the two-solitons, though the  $MSE$ s still need to be fully con-

verged. The cPINNs, where the conservation laws are applied to the  $MSE$ , did not work in this analysis because the strength of the conservation laws appears to be too low to enhance convergence. If the method eventually proves effective, we will undertake a more thorough investigation with substantial computational resources.

On the other hand, if we introduce a small perturbation, the friction term, into the equation, reasonable numerical convergence is observed well, and the identification is significantly improved by the other approaches. ‘Primarily, it works well when the friction term keeps a number of the conservation laws.

Our ultimate objective is to use the PINN technology to discover the most appropriate governing equation of the GRS based on various observational data or phenomenological considerations. If we encounter a problem similar to those discussed in this paper, it could be resolved using some of the minor perturbations covered in this study.

**Acknowledgments** The authors would like to thank Satoshi Horihata, Hiroshi Kakuhata, Ryu Sasaki, Filip Blaschke, and Paweł Klimas for their practical advice and valuable comments. N.S. and K.S. would like to thank all the conference organizers of QTS12 and Prof.Čestmir Burdík for their hospitality and many kind considerations. We sincerely appreciate the anonymous reviewers’ valuable comments and constructive suggestions, which have significantly improved the quality of this manuscript. K.S. was supported by Tokyo University of Science. A.N., N.S., and K.T. were supported in part by JSPS KAKENHI Grant Number JP23K02794.

## APPENDIX A: TECHNICAL SETUP OF THE PHYSICS-INFORMED NEURAL NETWORKS

Our analysis of the PINNs in this paper is based on a neural network consisting of 4 hidden layers, each containing 20 nodes. In order to fix the optimal parameters for both layers and nodes, here we solve the inverse problem of the ZK equation

$$u_t + \lambda_1 uu_x + \lambda_2 (\nabla^2 u)_x = 0 \tag{67}$$

for changing the number of layers or nodes. In Fig.15, we study the convergence property of the PINNs from 4 to 8 layers. This indicates that the result of the 6 layers is the best choice for convergence. Table XIII is the ability of the parameter prediction where the 4 layer looks better than the other number of the layers. The findings imply that selecting the layers is not as crucial

as one may think to achieve better solutions.

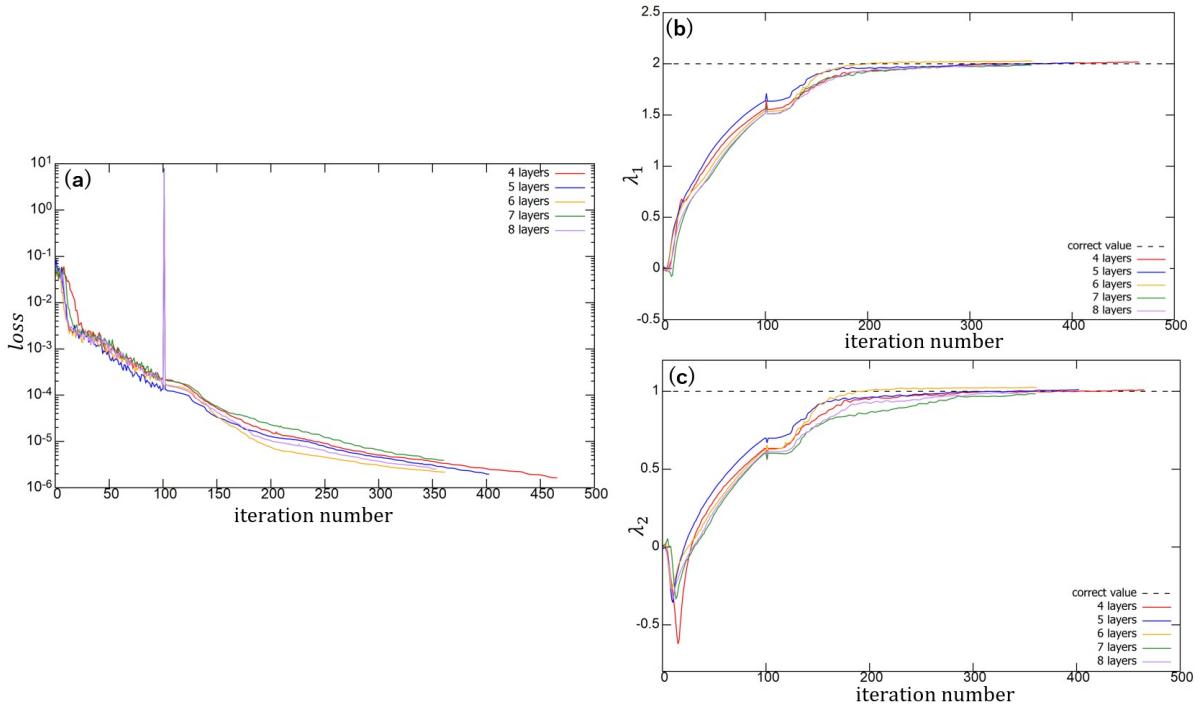


FIG. 15. The convergence of the loss function and the parameters of the ZK equation: (a) the *MSE*, (b) the predicted parameter of  $\lambda_1$ , (c) the predicted parameter of  $\lambda_2$ .

TABLE XIII. The accuracy of the parameter prediction.

layers	$\lambda_1$	$\lambda_2$
4	2.01547	1.00873
5	2.00811	1.01046
6	2.02570	1.02479
7	1.98557	0.98272
8	2.00094	0.99105

Next, we study the appropriate size of the training data in the inverse analysis. We employ the range of the coordinates set as  $x \in [-20, 20]$ ,  $y \in [-10, 10]$ ,  $t \in [0.0, 5.0]$  and the mesh number is set as  $N_x = 200$ ,  $N_y = 200$ ,  $N_t = 1000$ . The whole number of the training data becomes

$4 \times 10^7$  in this setup. Due to computational resource limits, we cannot use the whole data set for the PINN analysis; instead, we are forced to select the data’s collocation points at random. Surprisingly, Table XIV indicates that the PINNs do not lose their predictability even if they learn only 0.0125% of its whole data. In this paper, we always use 25000 points (0.0625% of its whole data) as the training data.

TABLE XIV. The predictability for the parameters  $\lambda_1, \lambda_2$  of the inverse analysis for the choice of the training data points (and the ratio to the whole data).

training points (ratio)	$\lambda_1$	$\lambda_2$
5000 (0.0125%)	2.00185	0.99356
10000 (0.025%)	2.01124	1.01236
15000 (0.0375%)	2.01065	1.00369
20000 (0.05%)	1.99789	1.00730
25000 (0.0625%)	2.01291	1.01996
30000 (0.075%)	2.00883	1.00784
35000 (0.0875%)	2.01950	1.01835

## REFERENCES

- 
- [1] N. J. Zabusky and M. D. Kruskal, “Interaction of ”solitons” in a collisionless plasma and the recurrence of initial states,” *Phys. Rev. Lett.* **15**, 240–243 (1965).
  - [2] Thomas Brooke Benjamin, J. L. Bona, and J. J. Mahony, “Model equations for long waves in nonlinear dispersive systems,” *Philosophical Transactions of the Royal Society of London. Series A, Mathematical and Physical Sciences* **272**, 47–78 (1972).
  - [3] V. Zakharov and E. A. Kuznetsov, “Three-dimensional solitons,” *Soviet Physics JETP* **29**, 594–597 (1974).
  - [4] Hiroshi Iwasaki, Sadayoshi Toh, and Takuji Kawahara, “Cylindrical quasi-solitons of the Zakharov-Kuznetsov equation,” *Physica D: Nonlinear Phenomena* **43**, 293–303 (1990).
  - [5] V. I. Petviashvili and V. V. Yan’kov, “Bilayer vortices in rotating stratified fluid,” *Dokl. Akad. Nauk SSSR* **267**, 825–828 (1982).
  - [6] Christian Klein, Svetlana Roudenko, and Nikola Stoilov, “Numerical study of Zakhavor-Kuznetsov equations in two dimensions,” *Journal of Nonlinear Science* **31**, 1–28 (2021).

- [7] D. H. Peregrine, “Calculations of the development of an undular bore,” *Journal of Fluid Mechanics* **25**, 321–330 (1966).
- [8] Takuji Kawahara, Keisuke Araki, and Sadayoshi Toh, “Interactions of two-dimensionally localized pulses of the regularized-long-wave equation,” *Physica D: Nonlinear Phenomena* **59**, 79–89 (1992).
- [9] Kh.O. Abdulloev, I.L. Bogolubsky, and V.G. Makhankov, “One more example of inelastic soliton interaction,” *Physics Letters A* **56**, 427–428 (1976).
- [10] J. Courtenay Lewis and J.A. Tjon, “Resonant production of solitons in the rlw equation,” *Physics Letters A* **73**, 275–279 (1979).
- [11] F. ter Braak, L. A. Ferreira, and W. J. Zakrzewski, “Quasi-integrability of deformations of the KdV equation,” *Nucl. Phys. B* **939**, 49–94 (2019), arXiv:1710.00918 [hep-th].
- [12] Marzia Parisi, Yohai Kaspi, Galanti. Eli, Daniele Durante, Scott J. Bolton, Levin. Steven M., Dustin R. Buccino, Leigh N. Fletcher, Folkner. William M., Tristan Guillot, Ravit Helled, Iess. Luciano, Cheng Li, Kamal Oudrhiri, and Michael H. Wong, “The depth of jupiter’s great red spot constrained by juno gravity overflights,” *Science* **374**, 964–968 (2021).
- [13] Akira Hasegawa and Kunioki Mima, “Pseudo-three-dimensional turbulence in magnetized nonuniform plasma,” *The Physics of Fluids* **21**, 87–92 (1978).
- [14] V. I. Petviashvili, “Red spot of jupiter and the drift soliton in a plasma,” *JETP Letters* **32**, 632 (1980).
- [15] Gareth Williams and Toshio Yamagata, “Geostrophic Regimes, Intermediate Solitary Vortices and Jovian Eddies,” *Journal of The Atmospheric Sciences - J ATMOS SCI* **41**, 453–478 (1984).
- [16] Jule G. Charney and Glenn R. Flierl, “Oceanic analogues of large-scale atmospheric motions,” *Evolution of physical oceanography* **504**, 548 (1981).
- [17] Yukito Koike, Atsushi Nakamura, Akihiro Nishie, Kiori Obuse, Nobuyuki Sawado, Yamato Suda, and Kouichi Toda, “Mock-integrability and stable solitary vortices,” *Chaos Solitons and Fractals: the interdisciplinary journal of Nonlinear Science and Nonequilibrium and Complex Phenomena* **165**, 112782 (2022), arXiv:2204.01985 [math-ph].
- [18] Maziar Raissi, Paris Perdikaris, and George Karniadakis, “Physics informed deep learning (part i): Data-driven solutions of nonlinear partial differential equations,” (2017), 10.48550/arXiv.1711.10561.
- [19] Maziar Raissi, Paris Perdikaris, and George Karniadakis, “Physics informed deep learning (part ii): Data-driven discovery of nonlinear partial differential equations,” (2017), 10.48550/arXiv.1711.10566.
- [20] M. Raissi, P. Perdikaris, and G.E. Karniadakis, “Physics-informed neural networks: A deep learning framework for solving forward and inverse problems involving nonlinear partial differential equations,” *Journal of Computational Physics* **378**, 686–707 (2019).
- [21] Maziar Raissi, Alireza Yazdani, and George Em Karniadakis, “Hidden fluid mechanics: Learning velocity and pressure fields from flow visualizations,” *Science* **367**, 1026–1030 (2020), <https://www.science.org/doi/pdf/10.1126/science.aaw4741>.
- [22] Steven L. Brunton, Bernd R. Noack, and Petros Koumoutsakos, “Machine learning for fluid mechanics,” *Annual Review of Fluid Mechanics* **52**, 477–508 (2020).

- [23] Teeratorn Kadeethum, Thomas M. Jorgensen, and Hamidreza M. Nick, “Physics-informed neural networks for solving nonlinear diffusivity and biot’s equations,” *PLOS ONE* **15**, 1–28 (2020).
- [24] Shengze Cai, Zhiping Mao, Zhicheng Wang, Minglang Yin, and George Em Karniadakis, “Physics-informed neural networks (pinns) for fluid mechanics: a review,” *Acta Mechanica Sinica* (2021), 10.1007/s10409-021-01148-1.
- [25] Kashinath K et al., “Physics-informed machine learning: case studies for weather and climate modeling,” *Phil.Trans.R.Soc.A* **379**, 20200093 (2021).
- [26] X. Jin, S. Cai, H. Li, and G.E Karniadakis, “NSFnets (NavierStokes flow nets): Physics-informed neural networks for the incompressible Navier-Stokes equations,” *Journal of Computational Physics* **426**, 109951 (2021).
- [27] Rahul Rai and Chandan K. Sahu, “Driven by data or derived through physics? a review of hybrid physics guided machine learning techniques with cyber-physical system (cps) focus,” *IEEE Access* **8**, 71050–71073 (2020).
- [28] Hao Wu, Feliks Nüske, Fabian Paul, Stefan Klus, Péter Koltai, and Frank Noé, “Variational Koopman models: Slow collective variables and molecular kinetics from short off-equilibrium simulations,” *The Journal of Chemical Physics* **146**, 154104 (2017), [https://pubs.aip.org/aip/jcp/article-pdf/doi/10.1063/1.4979344/14899047/154104.1\\_online.pdf](https://pubs.aip.org/aip/jcp/article-pdf/doi/10.1063/1.4979344/14899047/154104.1_online.pdf).
- [29] Georgios Kissas, Yibo Yang, Eileen Hwuang, Walter R. Witschey, John A. Detre, and Paris Perdikaris, “Machine learning in cardiovascular flows modeling: Predicting arterial blood pressure from non-invasive 4d flow mri data using physics-informed neural networks,” *Computer Methods in Applied Mechanics and Engineering* **358**, 112623 (2020).
- [30] Carlos Ruiz Herrera, Thomas Grandits, Gernot Plank, Paris Perdikaris, and Simone Sahli Costabal, Francisco andPezzuto, “Physics-informed neural networks to learn cardiac fiber orientation from multiple electroanatomical maps,” *Engineering with Computers* **38**, 3957–3973 (2022).
- [31] Kaan Sel, Amirmohammad Mohammadi, Roderic I. Pettigrew, and Roozbeh Jafari, “Physics-informed neural networks for modeling physiological time series for cuffless blood pressure estimation,” *npj Digital Medicine* **6**, 110 (2023).
- [32] S.M. Sivalingam, Pushpendra Kumar, and V. Govindaraj, “A chebyshev neural network-based numerical scheme to solve distributed-order fractional differential equations,” *Computers and Mathematics with Applications* **164**, 150–165 (2024).
- [33] S.M. Sivalingam, Pushpendra Kumar, and V. Govindaraj, “A novel optimization-based physics-informed neural network scheme for solving fractional differential equations,” *Engineering with Computers* **40**, 855–865 (2024).
- [34] Zhiwei Fang and Justin Zhan, “A physics-informed neural network framework for pdes on 3d surfaces: Time independent problems,” *IEEE Access* **8**, 26328–26335 (2020).
- [35] Francisco Sahli Costabal, Simone Pezzuto, and Paris Perdikaris, “Delta-pinns: Physics-informed neural networks on complex geometries,” *Engineering Applications of Artificial Intelligence* **127**, 107324

- (2024).
- [36] Shuning Lin and Yong Chen, “A two-stage physics-informed neural network method based on conserved quantities and applications in localized wave solutions,” *Journal of Computational Physics* **457**, 111053 (2022).
- [37] Ameya D. Jagtap, Ehsan Kharazmi, and George Em Karniadakis, “Conservative physics-informed neural networks on discrete domains for conservation laws: Applications to forward and inverse problems,” *Computer Methods in Applied Mechanics and Engineering* **365**, 113028 (2020).
- [38] Jun Li and Yong Chen, “A deep learning method for solving third-order nonlinear evolution equations,” *Communications in Theoretical Physics* **72**, 115003 (2020).
- [39] Yin Fang, Gang-Zhou Wu, Nikolay A. Kudryashov, Yue-Yue Wang, and Chao-Qing Dai, “Data-driven soliton solutions and model parameters of nonlinear wave models via the conservation-law constrained neural network method,” *Chaos, Solitons and Fractals* **158**, 112118 (2022).
- [40] J.C.Pu and Y.Chen, “Lax pairs informed neural networks solving integrable systems,” *J. Comput. Phys.* **510**, 113090 (2024).
- [41] Zhou Huijuan, “Parallel Physics-Informed Neural Networks Method with Regularization Strategies for the Forward-Inverse Problems of the Variable Coefficient Modified KdV Equation,” *J. Syst. Sci. Complex.* **37**, 511–544 (2024).
- [42] Shuning Lin and Yong Chen, “Physics-informed neural network methods based on miura transformations and discovery of new localized wave solutions,” *Physica D: Nonlinear Phenomena* **445**, 133629 (2023).
- [43] Zijian Zhou and Zhenya Yan, “Solving forward and inverse problems of the logarithmic nonlinear schrödinger equation with pt-symmetric harmonic potential via deep learning,” *Physics Letters A* **387**, 127010 (2021).
- [44] Juncai Pu, Jun Li, and Yong and Chen, “Solving localized wave solutions of the derivative nonlinear schrödinger equation using an improved pinn method,” *Nonlinear Dynamics* **105**, 1723–1739 (2021).
- [45] Z.W.Miao and Y.Chen, “Physics-informed neural networks method in high-dimensional integrable systems,” *Mod.Phys.Lett.B.* **36(1)**, 2150531 (2022).
- [46] Zijian Zhou, Li Wang, and Zhenya Yan, “Deep neural networks learning forward and inverse problems of two-dimensional nonlinear wave equations with rational solitons,” *Computers and Mathematics with Applications* **151**, 164–171 (2023).
- [47] Xue Peng, Yi-Wei Zhao, and Xing Lü, “Data-driven solitons and parameter discovery to the (2+1)-dimensional nlse in optical fiber communications,” *Nonlinear Dynamics* **112**, 1291–1306 (2024).
- [48] Li Wang, Zijian Zhou, and Zhenya Yan, “Data-driven vortex solitons and parameter discovery of 2d generalized nonlinear schrödinger equations with a pt-symmetric optical lattice,” *Computers and Mathematics with Applications* **140**, 17–23 (2023).
- [49] Siddhartha Mishra and Roberto Molinaro, “Physics informed neural networks for simulating radiative transfer,” *Journal of Quantitative Spectroscopy and Radiative Transfer* **270**, 107705 (2021).

- [50] Xingzhuo Chen, David J. Jeffery, Ming Zhong, Levi D. McClenny, Ulisses M. Braga-Neto, and Lifan Wang, “Using physics informed neural networks for supernova radiative transfer simulation,” (2022).
- [51] Yu Yang, Helin Gong, Shiquan Zhang, Qihong Yang, Zhang Chen, Qiaolin He, and Qing Li, “A data-enabled physics-informed neural network with comprehensive numerical study on solving neutron diffusion eigenvalue problems,” *Annals of Nuclear Energy* **183**, 109656 (2023).
- [52] Alexandr Sedykh, Maninadh Podapaka, Asel Saginalieva, Karan Pinto, Markus Pflitsch, and Alexey Melnikov, “Hybrid quantum physics-informed neural networks for simulating computational fluid dynamics in complex shapes,” *Machine Learning: Science and Technology* **5**, 025045 (2024).
- [53] Atsushi Nakamura, Kiori Obuse, Nobuyuki Sawado, Kohei Shimasaki, Junichiro Shimazaki, and Kouichi Toda, to be published (2024).
- [54] Gang-Zhou Wu, Yin Fang, Nikolay A. Kudryashov, Yue-Yue Wang, and Chao-Qing Dai, “Prediction of optical solitons using an improved physics-informed neural network method with the conservation law constraint,” *Chaos, Solitons and Fractals* **159**, 112143 (2022).
- [55] Zhao Chen, Yang Liu, and Hau Sun, “Physics-informed learning of governing equations from scarce data,” *Nature Communications* **12**, 1 (2021).
- [56] Pongpisit Thanasutives, Takashi Morita, Masayuki Numao, and Ken-ichi Fukui, “Noise-aware physics-informed machine learning for robust pde discovery,” *Machine Learning: Science and Technology* **4**, 015009 (2023).
- [57] Pongpisit Thanasutives, Takashi Morita, Masayuki Numao, and Ken-Ichi Fukui, “Adaptive uncertainty-penalized model selection for data-driven pde discovery,” *IEEE Access* **12**, 13165–13182 (2024).
- [58] Atsushi Nakamura, Kiori Obuse, Nobuyuki Sawado, Kohei Shimasaki, and Kouichi Toda, “Machine learning study through physics-informed neural networks: Analysis of the stable vortices in quasi-integrable systems,” *Journal of Physics: Conference Series* **2667**, 012079 (2023), <https://dx.doi.org/10.1088/1742-6596/2667/1/012079>.
- [59] L. A. Ferreira, G. Luchini, and Wojtek J. Zakrzewski, “The concept of quasi-integrability,” *AIP Conf. Proc.* **1562**, 43–49 (2013), arXiv:1307.7722 [hep-th].
- [60] E.A. Kuznetsov, A.M. Rubenchik, and V.E. Zakharov, “Soliton stability in plasmas and hydrodynamics,” *Physics Reports* **142**, 103–165 (1986).
- [61] Yohei Yamazaki, “Stability for line solitary waves of zakharov–kuznetsov equation,” *Journal of Differential Equations* **262**, 4336–4389 (2017).
- [62] Christian Klein, Jean-Claude Saut, and Nikola Stoilov, “Numerical study of the transverse stability of line solitons of the zakharov–kuznetsov equations,” *Physica D: Nonlinear Phenomena* **448**, 133722 (2023).
- [63] Thomas J. Bridges, “Universal geometric condition for the transverse instability of solitary waves,” *Phys. Rev. Lett.* **84**, 2614–2617 (2000).
- [64] Mathew A. Johnson, “The transverse instability of periodic waves in za-

- kharov–kuznetsov type equations,” *Studies in Applied Mathematics* **124**, 323–345 (2010), <https://onlinelibrary.wiley.com/doi/pdf/10.1111/j.1467-9590.2009.00473.x>.
- [65] Anne de Bouard, “Stability and instability of some nonlinear dispersive solitary waves in higher dimension,” *Proceedings of the Royal Society of Edinburgh: Section A Mathematics* **126**, 89–112 (1996).
- [66] P. Frycz and E. Infeld, “Spontaneous transition from flat to cylindrical solitons,” *Phys. Rev. Lett.* **63**, 384–385 (1989).
- [67] P. Frycz, E. Infeld, and J. C. Samson, “Spontaneous transition from flat to spherical solitons,” *Phys. Rev. Lett.* **69**, 1057–1060 (1992).
- [68] Katuhiko Goda and Yoshinari Fukui, “Numerical studies of the regularized long wave equation,” *Journal of the Physical Society of Japan* **48**, 623–630 (1980), <https://doi.org/10.1143/JPSJ.48.623>.
- [69] L. A. Medeiros and G. Perla Menzala, “Existence and uniqueness for periodic solutions of the benjamin-bona-mahony equation,” *SIAM Journal on Mathematical Analysis* **8**, 792–799 (1977), <https://doi.org/10.1137/0508062>.
- [70] D. Bhardwaj and R. Shankar, “A computational method for regularized long wave equation,” *Computers and Mathematics with Applications* **40**, 1397–1404 (2000).
- [71] Mehdi Dehghan and Rezvan Salehi, “The solitary wave solution of the two-dimensional regularized long-wave equation in fluids and plasmas,” *Computer Physics Communications* **182**, 2540–2549 (2011).
- [72] Mehdi Dehghan, Mostafa Abbaszadeh, and Akbar Mohebbi, “The use of interpolating element-free galerkin technique for solving 2d generalized benjamin-bona-mahony-burgers and regularized long-wave equations on non-rectangular domains with error estimate,” *Journal of Computational and Applied Mathematics* **286**, 211–231 (2015).
- [73] Thomas Brooke Benjamin, “The stability of solitary waves,” *Proceedings of the Royal Society of London. A. Mathematical and Physical Sciences* **328**, 153–183 (1972), <https://royalsocietypublishing.org/doi/pdf/10.1098/rspa.1972.0074>.
- [74] Yikai Chen, Hongli Xiao, Xiao Teng, Wenjun Liu, and Long Lan, “Enhancing accuracy of physically informed neural networks for nonlinear schrödinger equations through multi-view transfer learning,” *Information Fusion* **102**, 102041 (2024).
- [75] G.G. Sutyrin and T. Radko, “Why the most long-lived oceanic vortices are found in the subtropical westward flows,” *Ocean Modelling* **161**, 101782 (2021).